Probing inhibitory contacts between the regulatory and catalytic domains of CTP:phosphocholine cytidylyltransferase (CCT) using Transition metal ion Fluorescence Resonance Energy Transfer (tmFRET)

by

Aarati Sriram

B.Sc., Simon Fraser University, 2011

Thesis Submitted in Partial Fulfillment of the
Requirements for the Degree of
Master of Science

in the
Department of Molecular Biology and Biochemistry
Faculty of Science

SIMON FRASER UNIVERSITY

Summer 2014

Approval

Name: **Aarati Sriram**

Degree: **Master of Science**

Title: ***Probing inhibitory contacts between the regulatory and catalytic domains of CTP:phosphocholine cytidylyltransferase (CCT) using Transition metal ion Fluorescence Resonance Energy Transfer (tmFRET)***

Examining Committee: **Chair:** Dr. Frederic F. Pio
Associate Professor

Dr. Rosemary B. Cornell
Senior Supervisor
Professor

Dr. Lisa Craig
Supervisor
Associate Professor

Dr. Mark Paetzel
Supervisor
Professor

Dr. Edgar C. Young
Internal Examiner
Associate Professor

Date Defended: May 30, 2014

Partial Copyright Licence

Abstract

CCT catalyzes the rate-limiting step in phosphatidylcholine synthesis. CCT is activated when its lipid-induced amphipathic helix (domain M) binds to PC-deficient membranes and silenced when the auto-inhibitory motif (AI) within domain M binds helix αE in the catalytic domain. tmFRET was used to probe inter-domain interactions. Monobromobimane (donor) was conjugated to a cysteine engineered in αE or AI. My objective was to determine if a native di-histidine motif (^{89}HSGH^{92}) in the active site could function as a Cu^{2+} (acceptor) binding site. Fluorescence quenching occurred at Cu^{2+} concentrations above 10^{-5} M, but persisted when the binding site was compromised via histidine protonation, H89S mutation, or competition with CDP-choline. Cu^{2+}-quenching also persisted when domains M and C were dissociated by membrane binding. These results suggest that ^{89}HSGH^{92} is not an effective Cu^{2+} binding site and quenching was likely collisional. Future work will require engineering a di-histidine motif elsewhere in the catalytic domain.

Keywords: CTP:phosphocholine cytidylyltransferase (CCT); transition metal ion FRET (tmFRET); monobromobimane (mBBr); auto-inhibition; domain interactions; fluorescence quenching

To Karthik, Sriram, Jayashree and Rohit.

Thank you for all your love and support.

Acknowledgements

I would like to thank Dr. Rosemary B. Cornell for her guidance and support throughout the entire project and my committee members, Dr. Lisa Craig and Dr. Mark Paetzel for all their help and input. Thanks to all my wonderful lab mates. It was a pleasure to work with all of you. Special thanks to Ziwei Ding, Jaeyong Lee and Svetla Taneva for providing timely advice and teaching me so much. Thanks to Rahma Osman for being a great undergraduate assistant and helping me with data collection and analysis.

Thanks to my mom, dad and brother for their unwavering support, guidance and love. None of this would be possible without you. Special thanks to my dear husband, Karthik Ram, who supported me in every way possible during my studies. Thanks for all the love and encouragement. I would also like to extend my thanks to my in-laws for their love and support.

Table of Contents

List of Figures

List of Acronyms

AI	Auto-inhibitory
BBP	Biotin-binding protein
cAMP	Cyclic adenosine monophosphate
CCT	CTP:phosphocholine cytidylyltransferase
CNBD	Cyclic nucleotide-binding domain
DAG	Diacylglycerol
DEAE	Diethylaminoethyl
DMEM	Dulbecco's modified eagle medium
DMSO	Dimethylsulfoxide
DTT	Dithiothreitol
EDTA	Ethylenediaminetetraacetic acid
EQ	Equilibration
FBS	Fetal bovine serum
FRET	Fluorescence Resonance Energy Transfer
GCT	CTP:glycerol-3-phosphate cytidylyltransferase
GuHCl	Guanidine hydrochloride
HCN	Hyperpolarization-activated cyclic nucleotide-gated
IB	Inclusion body
IPTG	Isopropyl β-D-1-thiogalactopyranoside
k_{cat}	Overall enzymatic catalytic rate
K_m	Michealis-menton constant
LB	Lysogeny broth
mBBr	Monobromobimane
MBP	Maltose-binding protein
MS	Mass spectrometry
NLS	Nuclear localization signal
PA	Phosphatidic acid
PBS	Phosphate buffered saline
PC	Phosphatidylcholine
PCR	Polymerase chain reaction
PDB	Protein data bank

PE	Phosphatidylethanolamine
PG	Phosphatidylglycerol
PI	Phosphatidylinositol
PMSF	Phenylmethylsulfonyl fluoride
PMT	Photomultiplier tubes
PP_i	Pyrophosphate
PS	Phosphatidylserine
PVDF	Polyvinylidene fluoride
RFU	Relative fluorescence unit
SDS	Sodium dodecyl sulfate
SH	Src homology
SV	Simian virus
TBS	Tris-buffered saline
TE	Tris-EDTA
TEV	Tobacco etch virus
tmFRET	Transition metal ion FRET

Chapter 1.

Introduction

1.1. Protein regulation by auto-inhibition

Auto-inhibitory (AI) domains negatively regulate the function of a second, separable domain (functional domain) in a protein via specific intramolecular interactions. Auto-inhibition is an important regulatory mechanism that modulates protein function. An AI domain in a protein can be identified by analyzing the effect of deletion of a particular region on the protein's activity. If deletion confers constitutive activity, then this region is auto-inhibitory.

Auto-inhibition can occur through direct interference with the substrate-binding site in the functional domain. For example, Ca^{2+}/calmodulin-dependent protein kinase II is regulated by an auto-inhibitory mechanism in which a segment of the kinase acts as a pseudosubstrate and occupies the catalytic site. The binding of Ca^{2+}/calmodulin (ligand) to a target sequence on the AI domain, dissociates this inhibitory interaction (Yang and Schulman 1999). Auto-inhibition can also be achieved allosterically through indirect structural alteration of the catalytic domain. For example, Src kinases are kept inactive by intramolecular interactions between the SH3, SH2 and kinase domain (SH1). The phosphorylation of a C-terminal Tyr527 at the tail of the kinase domain reduces kinase activity whereas the phosphorylation of Tyr416 in the activation loop (kinase domain) results in full kinase activity. A rigid SH2-SH3 linker connecting the regulatory and kinase domain, generates a non-productive active site by changing the position of helix αC and the conformation of the activation loop in the kinase domain, impeding the protein from adopting the full active conformation (Cowan-Jacob, Fendrich et al. 2005). The inhibitory contact is broken upon dephosphorylation of the p-Tyr527. This introduces flexibility between the two domains and allows phosphorylation of Tyr416 in the activation loop.

Auto-inhibition is most commonly counteracted by displacement of the AI domain by another molecule (ligand or competing partner), resulting in the replacement of *intra*molecular interactions with *inter*molecular interactions (Pufall and Graves 2002). Alternatively, proteolysis of the inhibitory domain or post-translational modification can also disrupt inhibitory interactions (Pufall and Graves 2002).

My thesis focuses on a key regulatory enzyme in phospholipid metabolism that is regulated by auto-inhibition, CTP:phosphocholine cytidylyltransferase (CCT). In CCT, auto-inhibition is achieved by direct inter-domain contacts between the catalytic and regulatory domains. The activating ligand that dissociates this inhibitory interaction is a cell membrane. The succeeding sections will provide a brief review of CCT and its auto-inhibitory mechanism.

1.2. CTP:phosphocholine cytidylyltransferase (CCT)

1.2.1. Role of CCT in PC metabolism

Phosphatidylcholine (PC) is the most abundant phospholipid in mammalian cells and is a major lipid component of the eukaryotic cell membranes (Jackowski and Fagone 2005). In addition to contributing to the maintenance of the bilayer structure of membranes, PC is also the main component of pulmonary surfactant (Goerke 1998) and is a source for important lipid second messengers, such as diacylglycerol (DAG), phosphatidic acid and arachidonic acid. These products are important in the transduction of intracellular signals and regulate cellular events, such as cell growth and differentiation (Exton 1990).

In eukaryotic organisms, PC is most commonly synthesized via the CDP-choline or Kennedy pathway (Kent 1997), which transforms dietary choline into PC in three steps (Figure 1.1A). In the first step, choline is phosphorylated by choline kinase to form phosphocholine. The enzyme, CTP:phosphocholine cytidylyltransferase (CCT) then catalyzes the transfer of cytidine 5'-mono-phosphate (CMP) from CTP to phosphocholine to produce CDP-choline and pyrophosphate (PP_i) (Figure 1.1B). In the final step, CDP-choline reacts with DAG to yield PC; this reaction is catalyzed by choline

phosphotransferase. CCT catalyzes the rate-limiting and regulatory step in the synthesis of PC.

Alternatively, PC can also be synthesized in the hepatic cells of animals by the successive methylation of phosphatidylethanolamine (PE) (Kent 1997). Similarly in bacteria, PC is synthesized solely by the methylation of PE, whereas yeast can utilize either pathway.

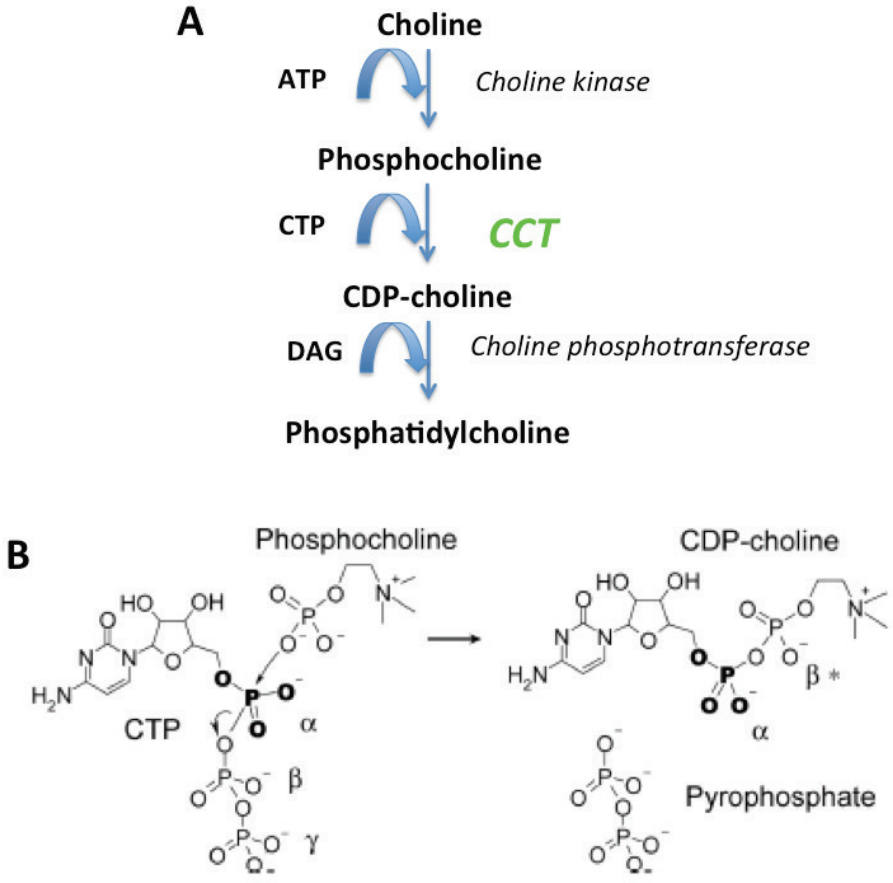

Figure 1.1. CDP-choline pathway and CCT catalyzed reaction.
(A) The 3-step CDP-choline pathway catalyzed by choline kinase, CCT, and choline phosphotransferase. (B) The CCT-catalyzed nucleophilic displacement reaction for CDP-choline synthesis from phosphoholine and CTP. The phosphocholine phosphate becomes the β*-phosphate in the product . Figure 1.1B is from (Lee, Johnson et al. 2009), Figure 1B.

1.2.2. Characterization and localization of CCT

Kennedy and Weiss were the first ones to discover CCT when they were studying the synthesis of PC in extracts of rat liver. The Kennedy laboratory showed that the enzyme was present in both soluble and membrane-bound forms (Wilgram and Kennedy 1963). Fiscus and Schneider showed that lipids were required to activate the cytosolic form (Fiscus and Schneider 1966). Hence, CCT is termed an amphitropic enzyme, meaning that the protein can interconvert between an inactive soluble form and an active membrane-bound form. The enzyme's tendency to aggregate and lose activity, delayed its purification for thirty years. Later, Weinhold and his colleagues were successful in purifying mammalian CCT from rat liver by adding detergents and lipids and treating the soluble fraction as a membrane enzyme (Weinhold, Rounsifer et al. 1986)

The first CCT cDNA was cloned from yeast (Tsukagoshi, Nikawa et al. 1987) and the second from rat liver (Kalmar, Kay et al. 1990). The cloning of CCTs from various organisms as well as genome sequencing has now provided us with many CCT sequences. There are three human isoforms of CCT: α, β_1 and β_2. These isoforms are identical in their catalytic domains, but differ in their regulatory regions (Jackowski and Fagone 2005). While the beta forms are cytoplasmic and show tissue-selective expression, the alpha form is ubiquitously expressed and is found in both the nucleus and the cytoplasm (Jackowski and Fagone 2005). Rat CCTα was used for all the experiments discussed in this thesis, and is simply referred to as CCT.

1.2.3. The domain structure of CCT

CCT is a homodimer; each monomer is composed of 367 amino acids. CCT consists of four functional domains (Figure 1.2): the N-terminal domain (residues 1-75), the catalytic domain (residues 75-236), the membrane-binding domain (residues 236-312) and the phosphorylation domain (residues 315-367). The head region houses domain N and the catalytic domain, and the structurally loose regulatory tail is composed of domains M and P.

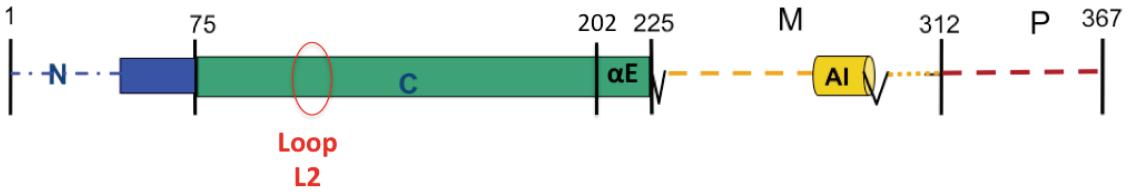

Figure 1.2 Domains of CCT.
CCT has 4 domains: N, C, M and P (N-terminal, Catalytic, Membrane-binding and Phosphorylation). The dotted lines show disordered regions. Regions important for regulating CCT activity are shown: mobile loop L2, helix αE and the auto-inhibitory (AI) motif.

Domain N contains a nuclear localization signal (NLS) at the N-terminus (residues 8-28), which directs the enzyme to the nucleus (Wang, MacDonald et al. 1995). The solved crystal structure of CCT236 (PDB: 3HL4), truncated at the end of the catalytic domain, shows that the C-terminal half of domain N (residues 40-75) sits on top of the catalytic domain and contributes to dimer interactions and stabilizes folding (Figure 1.3) (Lee, Johnson et al. 2009). The first 39 residues of domain N are not visible in this crystal structure. Secondary structure algorithms predicted that this region is disordered.

Domain C is responsible for catalysis. This domain is highly conserved across numerous species and among members of the cytidylyltransferase superfamily, which includes CCT, CTP:glycerol-3-phosphate cytidylyltransferase (GCT) from *Bacillus subtilis* and the eukaryotic CTP:phosphoethanolamine cytidylyltransferase (PDB: 3ELB). The structures of these three enzymes have been solved (Weber, Park et al. 1999, Pattridge, Weber et al. 2003, Lee, Johnson et al. 2009), and are homologous. In addition, there are two highly conserved motifs found within the catalytic domains of all cytidylyltransferases: HXGH (Veitch and Cornell 1996, Park, Gee et al. 1997) and RTEGIST(S/T) (Pattridge, Weber et al. 2003, Lee, Johnson et al. 2009). It is likely that these enzymes employ the same catalytic mechanism, due to the high similarity in their amino acid sequences and structure.

The solved crystal structure of CCT236 shows that the catalytic domain contains an α/β protein fold (Figure 1.3) with five parallel β strands in a twisted sheet: β1-β5, surrounded by six α helices: αA, αB, αC, αD, αL and αE (Lee, Johnson et al. 2009). The dimerization interface involves helix αA, αC, αE in the catalytic domain and the N-cap

segment (residues 40-75 in region N). The product, CDP-choline is bound to the active site pocket at the base of the β-sheet in each monomer of the CCT dimer.

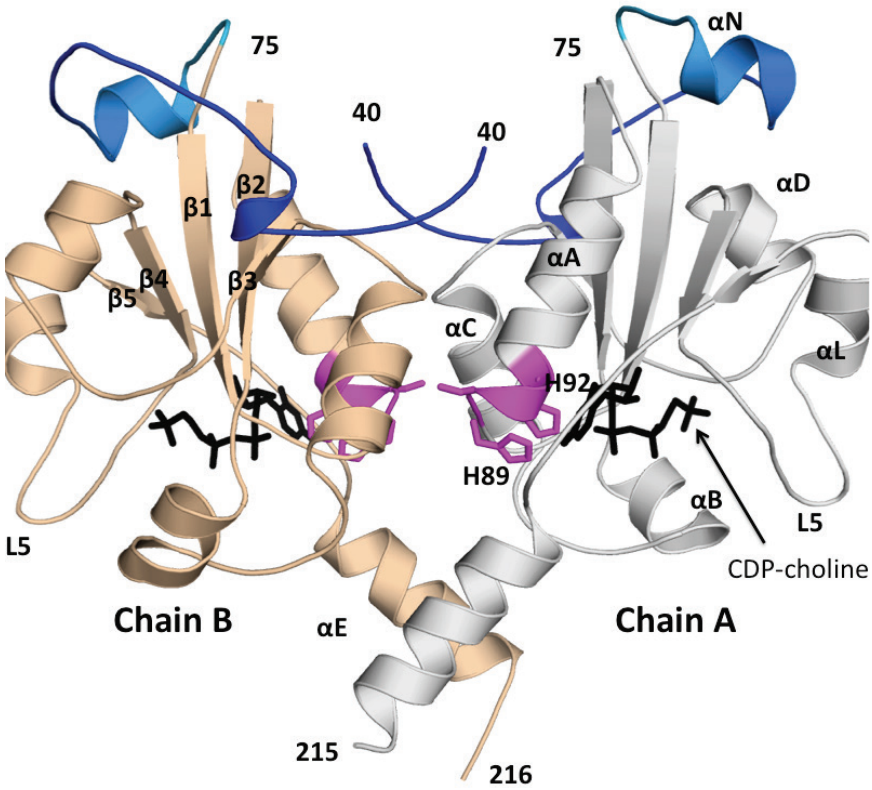

Figure 1.3 The tertiary structure of CCT236.
This structure shows domain N and the catalytic domain of CCT236. Chain A consists of residues 40-215 and chain B, residues 40-216. Domain N (residues 40-75) is shown in blue. Each subunit consists of 5 β sheets (β1-β5) and six α-helices (αA, αB, αC, αD, αL and αE). The ^{89}HSGH^{92} motif in also shown (magenta). The figure is modified from (Lee, Johnson et al. 2009), Figure 3A.

The regulatory domain of CCT, containing **domain M,** is responsible for membrane binding and enzyme activation (Craig, Johnson et al. 1994). Membrane binding of domain M is regulated by lipid composition; anionic lipids and diacylglycerol stabilize the membrane-bound form (Cornell and Northwood 2000). Circular dichroism analyses have revealed that in the presence of anionic lipid vesicles, domain M transitions from a random coil to a long amphipathic α-helix (Taneva, Johnson et al. 2003), with an asymmetric distribution of polar and hydrophobic residues (Dunne, Cornell et al. 1996). The nonpolar face of the helix contains 18 hydrophobic residues that facilitate membrane intercalation. The polar/nonpolar interface in the helical conformation is rich in arginine and lysine residues. These positively charged residues

interact electrostatically with negative charges on the membrane surface (Johnson, Xie et al. 2003)

In animal CCTs, the N-terminal of domain M is disordered, highly positively charged and has a low hydrophobicity whereas, the C-terminal end has net negative charge and is more hydrophobic. Unlike the catalytic domain, domain M shows very little conservation of sequence across phyla, with the exception of the extreme N-terminus and a C-terminal conserved 22-mer motif in metazoan CCTs (Ding, Taneva et al. 2012) (Figure 1.4A). The conserved 22-mer segment has a distinct spacing of hydrophobic and polar residues. As will be discussed later (section 1.2.6), this 22-mer segment, also known as the auto-inhibitory (AI) motif, is a key contributor to regulation of CCT activity. Domain M also acts as an auto-inhibitory domain in the soluble form, via direct interaction of the 22-mer AI motif with the catalytic domain. This inhibition is relieved upon the binding of domain M to membranes (Friesen, Campbell et al. 1999).

Vertebrate CCT possess a distinct 11-mer motif within domain M that is repeated four times in tandem (residues 256-288) and this sequence shares similarity with the 11-mer motif found in α-synuclein, the Parkinson's disease protein (Ding, Taneva et al. 2012) (Figure 1.4B). This motif is unique to vertebrate CCT and synucleins and in α-synuclein this sequence helps promote membrane interactions.

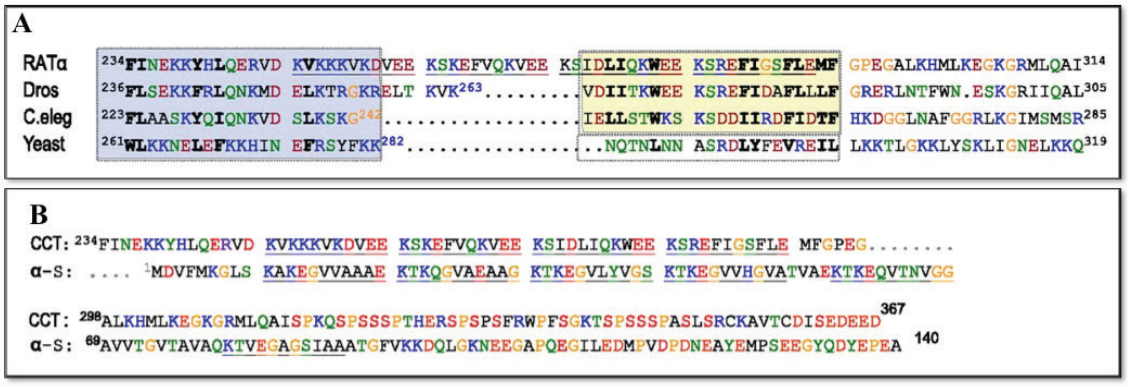

Figure 1.4 Sequence alignment of domain M of CCT.
Figure (A) shows region M of the following CCts: Ratα, *D. melanogaster*, *C. elegans* and Yeast (*S. cerevisiae*). The blue box shows the positively charged N-terminal segment and the yellow box shows the regulatory 22-mer segment. (B) Sequence alignment of rat CCTα with human α-synuclein. In both figures the 4 11-mer motifs are underlined. Amino acid color code: red-acidic, blue-basic, green-hydrophilic, black-hydrophobic and orange-glycine/proline residues. This figure is from (Ding, Taneva et al. 2012), Figure 1A & C.

Domain P, the phosphorylation domain, is 55 residues long in the alpha isoform, unstructured, and highly accessible to proteases (Bogan, Agnes et al. 2005). This domain is rich in serine and proline residues and of these, 16 serine residues in the C-terminal end can be phosphorylated in cells (MacDonald and Kent 1994). The presence of seven prolines led to the hypothesis that proline-directed kinases were responsible for CCT phosphorylation. It has been proposed that the phosphorylation state of CCT regulates its activity and membrane association. In the inactive soluble form, domain P is highly phosphorylated whereas, in the active membrane-bound form, the enzyme is dephosphorylated (Kent 1997). Domain P has poor sequence conservation across species.

1.2.4. CCT catalysis

CCT catalyzes the formation of CDP-choline (head group donor) using phosphocholine and CTP as substrates. The formation of CDP-choline occurs via direct nucleophilic attack of the α-phosphate of CTP by the phosphoryl oxygen of phosphocholine (Figure 1.1B). Since both GCT and CCT are highly similar in structure and share similar k_{cat} and K_m values, GCT was initially used as a model to understand the mechanism of catalysis in cytidylyltransferases. The two key sequence motifs,

^{83}GIFDLFHSGH^{92} and ^{196}RTEGISTS^{203} are highly conserved in the catalytic domains of both GCT and CCT. The HXGH motif is also found in class I aminoacyl tRNA synthetases, which are also members of the nucleotidyltransferase superfamily (Bork, Holm et al. 1995). This sequence has been shown to stabilize a pentavalent transition state in tRNA synthetases (Leatherbarrow, Fersht et al. 1985). Similarly, the HSGH motif located at the start of helix αA is thought to participate in CTP binding and pentavalent transition state stabilization in the CCT reaction (Bork, Holm et al. 1995, Veitch and Cornell 1996).

The solved structure of mammalian CCT236 revealed that many conserved residues in the active site contribute to interactions with the CDP group and phosphocholine (Lee, Johnson et al. 2009). The cytosine base of CDP-choline forms direct contacts with the ^{196}RTEGISTS^{203} motif in loop L6. The side chains of Asp169 at the base of β4 and Arg196 in loop L6 make contact with the ribose 2'-hydroxyl. The active site residues Lys122, His168 and Tyr173 form hydrogen-bonding interactions with phosphocholine and are likely involved in positioning this substrate for nucleophilic attack on the α-phosphate of CTP. The N-ε2 of His92 in the ^{89}HSGH^{92} motif contacts an exo-oxygen of the α-phosphate of CDP-choline and His89 is likely to bind to the β and γ phosphates of CTP, by analogy to its analog in the GCT-CTP complex (Weber, Park et al. 1999). Mutagenesis of these key residues revealed their role in catalysis. For example, mutations of either histidines to asparagine in the HSGH motif of CCT resulted in decreased k_{cat}/K_m (Veitch, Gilham et al. 1998). Similarly mutation of Lys-122 resulted in a large decrease in k_{cat}/K_m for CTP (Helmink, Braker et al. 2003). To date, the precise function of each of these residues during the progress of the reaction is not known.

1.2.5. Regulation of CCT activity by membrane binding and phosphorylation

Membrane binding and dephosphorylation are two modes of regulation that are responsible for triggering activation of the enzyme. CCT responds to a decrease in membrane PC content by translocating to the target membrane and binding to it. The membrane-bound form of the enzyme has much higher activity than the soluble form. *In vitro* studies with CCT and small unilamellar vesicles have shown that anionic

phospholipids (PI, PS, PG and PA) are potent activators of CCT and type II lipids with small head groups (unsaturated PE or DAG) activate CCT, but to a lesser degree (Cornell and Northwood 2000). The small head groups create surface voids and impose negative curvature strain on the bilayer. The insertion of CCT's membrane binding amphipathic helix (m-AH), helps relieve the lipid packing stress (Davies, Epand et al. 2001). Therefore, membrane properties such as lipid packing defects, negative curvature strain and changes in membrane lipid composition promote CCT insertion and activation. Binding to membranes is a two-step process: 1) electrostatic adsorption followed by 2) hydrophobic interactions, which involves intercalation into the non-polar lipid core (Cornell and Northwood 2000). The negatively charged phospholipids in the target membrane attract positively charged basic amino acids on domain M. Once CCT is docked onto a membrane, the hydrophobic face of the amphipathic helix inserts into one leaflet whereas the polar face is exposed to the aqueous environment.

Phosphorylation of domain P antagonizes membrane binding. There is a strong negative correlation between the phosphorylation state of CCT and membrane association. In vitro studies have revealed that phosphorylation of serines in the C-terminal end of the enzyme decreases membrane affinity (Arnold, DePaoli-Roach et al. 1997), and this may operate by a charge-repulsion mechanism (Chong, Taneva et al. 2014). Dephosphorylation or addition of negatively charged activating lipids would by-pass the repulsion. Interestingly, mutant CCT incapable of phosphorylation did not affect PC biosynthesis when expressed in CHO-58 cells, which lacks functional endogenous CCTα at the non-permissive temperature (Wang and Kent 1995). Hence, the importance of phosphorylation in CCT regulation is elusive.

1.2.6. CCT silencing mechanism, circa 2011.

The membrane-binding domain involved in activation also interacts closely with the catalytic domain in the enzyme's soluble state to inhibit activity (Friesen, Campbell et al. 1999). In cultured cells, oleic acid is commonly used to induce wild type CCT translocation to membranes and activation. Wang and Kent showed that upon deletion of M, oleic acid-induced translocation was not required for active CCT and PC synthesis (Wang and Kent 1995). The constitutive activity of purified CCT236, truncated at the

start of domain M, was later demonstrated (Friesen, Campbell et al. 1999). However, the maximal activity of CCT236 is only one-third the activity of full-length CCT. Thus, domain M contributes both positively and negatively to the regulation of the enzyme.

To study the features of domain M critical for silencing and to probe head and tail interactions, Ding and colleagues created chimeric proteins that contained the catalytic region of rat CCTα fused to the regulatory tail of CCTs from *C. elegans*, *Drosophila*, *S. cerevisae* or *α-synuclein* (Ding, Taneva et al. 2012). Their analyses indicated that a 22-mer segment (residues 272-293) in the C-terminal end of domain M conserved only in metazoan CCTs has an important regulatory role. This segment, also known as the auto-inhibitory (AI) motif, is an effective silencer of the rat catalytic domain. Deletion of this segment (CCT-Δ22) resulted in ineffective silencing and increased the lipid independent activity by 10-fold (similar to CCT236). In addition to this, the enzyme also had a weakened affinity for anionic lipid vesicles, suggesting that the hydrophobic residues in the 22-mer segment are involved in lipid interaction and membrane intercalation. The AI motif is the most structured segment in the flexible domain M (Huang, 2011).

To probe the sites of contact between domain M and the catalytic domain, Huang and colleagues conjugated a photoactivatable, biotin-tagged cross-linker (BBP) to single-cysteine variants in domain M and identified UV-dependent cross-links to other domains by digesting the labeled CCTs, isolating the biotinylated species and identifying them using mass spectrometry methods (Huang, 2011). Interestingly, each conjugated site in domain M forged cross-links to the same set of peptides in domain C. These peptides form part of the active site. The docking site for domain M segments was mapped to a pair of amphipathic helices (αE) of the CCT dimer, at the base of the active site. These contacts were broken upon membrane binding. Hydrogen/deuterium (H/D) exchange MS analyses further confirmed helix αE as the docking site for domain M. Fluorescence anisotropy analyses suggested that domain M's silencing mechanism does not involve a classical lock-and-key contact of rigid structure with the active site. Rather domain M appeared to be in a malleable, fluctuating state in which small islands of ordered structure are induced by forming multiple transient alternating contacts with helix αE (Figure 1.5).

We needed additional evidence for the silencing interaction between domain M and the catalytic domain. Hence, we turned to a FRET-based approach to achieve this goal.

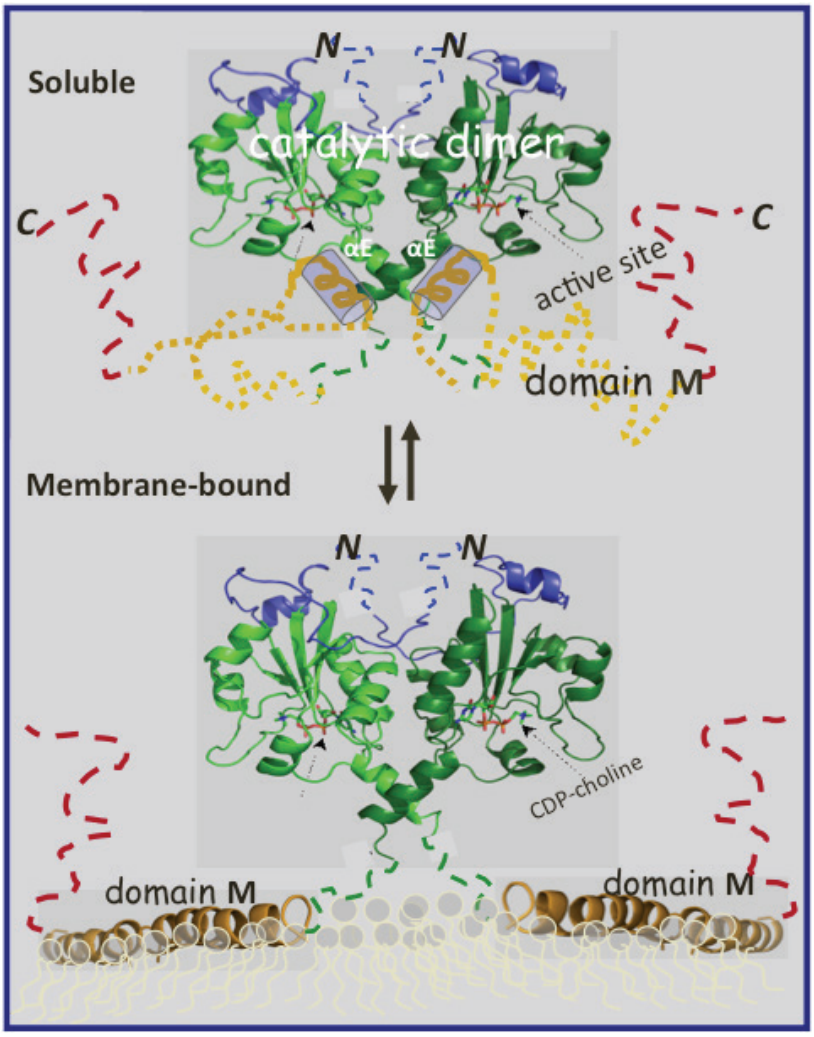

Figure 1.5 CCT reversible binding to membranes involves positive and negative roles for domain M.
In the inactive state, portions of domain M interact with the C domain to silence catalysis. Membrane-binding dissociates this interaction, and domain M folds into an amphipathic helix and inserts into the bilayer, activating CCT.

1.3. Fluorescence Resonance Energy Transfer (FRET)

Fluorescence resonance energy transfer (FRET) occurs when excitation energy is transferred from a donor fluorophore (excited state) to an acceptor fluorophore (ground state) through dipole-dipole coupling. It is a useful tool for measuring interatomic

distances and conformational changes in biological molecules. The efficiency of energy transfer (E) is inversely proportional to the sixth power of the distance. Hence, FRET is extremely sensitive to changes in distances. FRET results in a decrease in the donor's fluorescence intensity due to quenching by the acceptor. The distance (r) between the donor and acceptor can be calculated by measuring the FRET efficiency (E) and R_o using the equation: $E = 1/(1 + (r/R_o)^6))$, where R_o is the distance at which FRET efficiency is 50%.

In traditional FRET the R_o values are typically 30-60 Å (Lackowicz, 2006). The primary conditions for FRET include: a) the emission spectrum of the donor should overlap with the absorbance spectrum of the acceptor, b) the donor and acceptor should be within an effective distance and c) effective orientation of the donor/acceptor dipoles (Lackowicz, 2006). Fluorescence labels can be introduced into proteins by covalent attachment to native or engineered cysteines or using thiol-reactive fluorescence probes.

1.3.1. Introduction to transition metal ion FRET (tmFRET)

Classical FRET methods are sometimes not useful for studying intramolecular movements in proteins due to the large R_o values of FRET pairs (30-60 Å) and their long flexible linkers (10-15 Å) (J.W., Puljung et al. 2009). These distances are larger than many proteins. An improved method called transition metal ion FRET (tmFRET) uses colored transition metal ions such as Ni^{2+} or Cu^{2+} as acceptors and works over shorter distances. These metal ion acceptors are bound to di-histidines spaced one turn away on an α-helix within the protein. The advantages of using this technique are as follows: a) works over shorter distances (5-20 Å), b) uses small dyes with no linkers, c) has low fluorophore orientation dependence, d) can use multiple acceptors to probe the same donor position and e) FRET can be turned on and off by simple addition or removal of metals as they are noncovalently bound (Taraska, Puljung et al. 2009). This approach was used successfully to examine inter-domain movements coincident with cAMP binding to a cyclic nucleotide gated ion channel (J.W., Puljung et al. 2009), conformational changes in maltose-binding protein (MBP) (Yu, Wu et al. 2013) and to assess movements between two domains of the AAA+ ClpX ATPase in two conformational states (Stinson, Nager et al. 2013).

1.3.2. Monobromobimane and transition metal ions

The large size of the fluorophores and their long flexible linkers position the dye far from the backbone of the protein, increasing the conformational space of the dye (Taraska, Puljung et al. 2009). As a result, the structure of the protein and the changes in the protein's backbone position may be inaccurately represented, complicating the interpretation of FRET results. Therefore, Taraska and colleagues used a small, Tryptophan-sized fluorescent dye called monobromobimane (mBBr). Bimane is fluorescent whereas mBBr remains nonfluorescent until conjugated due to internal quenching by the Br. The dye has a cysteine-reactive methyl bromide linker that allows it to react with cysteine residues on the protein and displace Br^- (Figure 1.6).

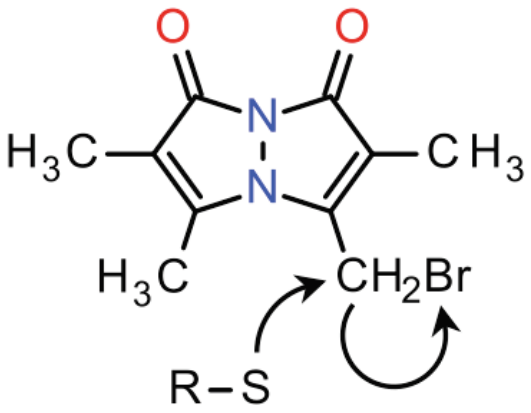

Figure 1.6 Monobromobimane and protein (cys) conjugation pathway.
Monobromobimane has a cysteine-reactive bromo-methyl group. HBr is eliminated in the formation of a stable thioether bond with the protein.

Transition metals such as Ni^{2+}, Cu^{2+} and Co^{2+} absorb wavelength from visible light causing them to be colored. The absorbance spectra for colored transition metal ions are broad and they have low extinction coefficients (Yu, Wu et al. 2013). Due to their short R_o values, they can act as FRET acceptors only at short distances. The weak absorbance spectra of the transition metal ions (Cu^{2+} and Ni^{2+}) overlap with the emission spectrum of bimane (Figure 1.7). The tm-FRET method provides more sensitive detection of close-range distances than traditional FRET-pairs.

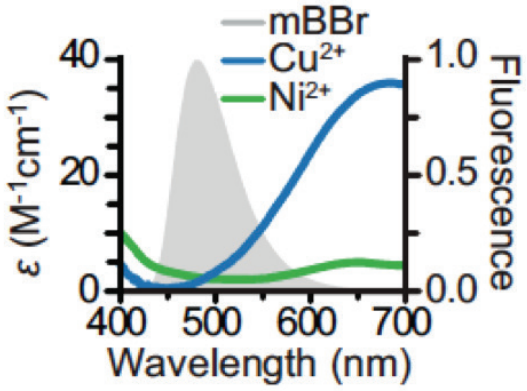

Figure 1.7 Overlap of emission spectrum of mBBr and absorbance spectra of Cu^{2+} and Ni^{2+}.

The emission spectrum of mBBr reacted with glutathione overlaps with the absorbance spectra of the transition metals, Cu^{2+} and Ni^{2+} bound to a synthetic peptide (ACAAKAAAKHAAAHKA). This figure is from (Taraska, Puljung et al. 2009), Figure 1A.

1.4. Overview of objectives

The main objective of my master's project was to use tm-FRET to probe the inhibitory interactions between the AI motif and helix αE and to assess average distances between the two sites. To achieve this goal, I first carried out a proof-of-principle trial to test the utility of a native di-histidine motif in the active site of CCT as a metal ion-binding site or FRET acceptor.

I conjugated mBBr (donor) to a single engineered cysteine at residue 207 in helix αE or residue 295 in the AI turn via sulfhydryl targeting. Copper (Cu^{2+}), which coordinated to a pair of native histidines in the ^{89}HSGH^{92} motif the active site, served as the acceptor. Fluorescence quenching experiments were performed upon addition of increasing concentrations of Cu^{2+}. If two sites in CCT are interacting and are within tmFRET distance, the fluorophore's fluorescence intensity will decline upon addition of transition metal ion. The motivation behind this work was to establish if a close correlation between the AI docking on αE and the silencing function exists.

Chapter 2. Methods and Materials

2.1. Materials

The pAX142 expression vector and COS-1 cells were gifts from Dr. Robert Kay (Terry Fox laboratory, BC Cancer research, UBC). PureLinkTM HiPure Plasmid Filter Maxiprep kit, restriction enzymes (Kpn1, SalI and NdeI), Dulbecco's Modified Eagle Medium, 5% Fetal bovine serum, Penstrep and AcTEV protease, Isopropyl β-D-1-thiogalactopyranoside (IPTG) and DH5α E. coli competent cells were purchased from Invitrogen and tissue culture flasks were from BD-Falconware. Spectra/Por 7 dialysis membranes (35 kDa MWCO) were from Spectrum Labs Inc. QIAprep® Spin Miniprep Kit for plasmid purification and Ni-NTA Agarose beads were purchased from Qiagen. The fluorescent dye Monobromobimane (mBBr) 25mg, catalog number M-1378 was purchased from Life Technologies. The oligonucleotide primers were purchased from Integrated DNA Technologies (IDT). 10X PCR buffer, Pfu DNA polymerase, 10mM dNTP and DpnI were purchased from Thermo Scientific. The pET-24a(+) expression vector, RosettaTM and NovaBlue competent cells were from Novagen. Phusion DNA polymerase was purchased from Fisher. The antibiotics, kanamycin and chloramphenicol were purchased from Sigma-Aldrich.

2.2. Methods for expression, purification, labeling and fluorescence analysis of CCT367-T207C in pAX142

2.2.1. pAX142 expression vector

pAX142 is an expression vector derived from pAX114 (Kay & Humphries, 1991), which has an elongation factor-1α promoter instead of a human cytomegalovirus promoter. The pAX142 vector has an SV40 origin of replication, which allows for its rapid replication to high copy number when introduced into SV40 transformed COS-1 cells. These cells express large SV40 T antigens, which bind to the SV40 origin of replication on pAX142 and allow host DNA polymerases to replicate the vector. This ultimately results in high expression of the encoded protein. The pAX142 vector also contains a pUC19 origin of replication for replication in *E.coli*, and a SupF suppressor tRNA which allows rescue of the amber mutation in the antibiotic resistance genes of the P3 element carried in *E.coli* strain DH5α-P3 (a biosafety design).

2.2.2. Construction and plasmid DNA preparation of pAX142-His(TEV)-CCT367-T207C

Construction of pAX142-His(TEV)-CCT367-T207C. I assisted Ziwei Ding with the preparation of pAX142-His(TEV)-CCT367-T207C. This construct consists of the COS-1 cell expression vector pAX142 with full-length rat CCTα containing a single cysteine at codon 207. pAX142-His(TEV)-CCTα (Dennis, Taneva et al. 2011) was digested with KpnI and the 2778 bp fragment was ligated into the 1440 bp fragment of pAX142-His(Xa)-CCT367-T207C (Huang, Taneva et al. 2013) which had also been digested with KpnI (Figure 2.1). The Factor Xa site was replaced with the tobacco etch virus (TEV) protease site just upstream of the His-tag. Factor Xa cleaves in the CCTα sequence and is not strictly confined to the site in the linker, whereas the TEV site, cleaves specifically at the linker site (Taneva, Dennis et al. 2008).

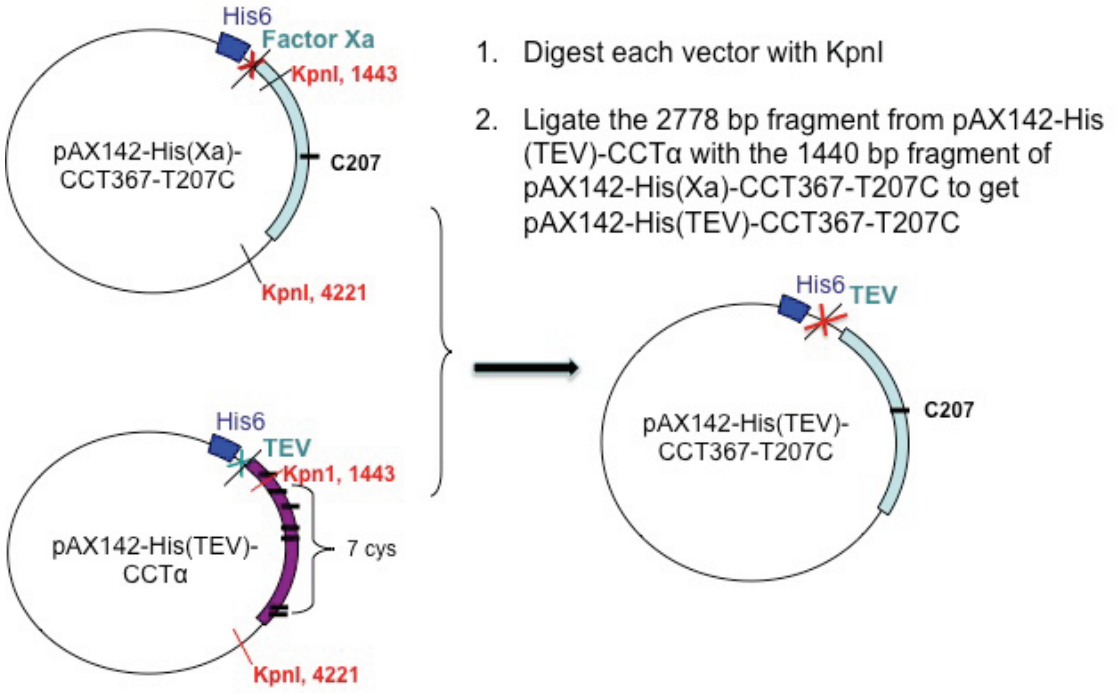

Figure 2.1 Construction of pAX142-His(TEV)-CCT367-T207C.
The full-length pAX142-His(TEV)-CCTα was digested with KpnI. The resulting 2778 bp fragment was then ligated with the 1440 bp fragment from pAX142-His(Xa)-CCT367-T207C, which was also digested with KpnI, as shown. The Factor Xa site was replaced with a TEV site upstream of the His-tag.

Plasmid DNA preparation. Plasmid DNA was isolated from *E.coli* cells using the PureLink™ HiPure Plasmid Maxiprep Kit, which employs the alkaline lysis method followed by DNA precipitation using centrifugation and an anion-exchange resin to purify the plasmid DNA. This kit allows for the purification of 500-850 µg of high-quality plasmid DNA from 100-200 ml of overnight *E.coli* cultures.

2.2.3. Transfection and Harvesting of COS-1 cells,

COS-1 cells. COS-1 cells are fibroblast-like cells derived from the African green monkey kidney. These cells are transformed with a mutant form of the Simian Virus 40 (SV40), which has a WT version of the viral replicase (virus T-antigen) but has a defect in genomic replication. The introduction of any vector containing an SV40 origin of replication into COS-1 cells results in rapid replication of the vector to the order of several hundred thousand copies per cell. COS-1 cells are used for high-level expression of mammalian proteins that require post-translational modifications not performed in the commonly used bacterial expression systems (Gluzman 1981).

The procedures for transfection, harvesting and purification of the expressed His-CCT were adapted from published protocols (Xie, Smith et al. 2004, Taneva, Dennis et al. 2008).

COS-1 cell transfections. COS-1 cells were maintained by passaging 1/10 every three days in Dulbecco's Modified Eagle Medium (DMEM) supplemented with 5% (v/v) Fetal Bovine Serum (FBS). These cells were subcultured 24 h preceding transfection, and plated at a density of 1.0 x 10^6 cells/10 cm dish or 2.5 x 10^6 cells/15 cm dish. The plates were first washed with TS buffer (140 mM NaCl, 25 mM Tris (pH 7.5), 5 mM KCl, 0.5 mM Na_2HPO_4, 1 mM $MgCl_2$, 1 mM $CaCl_2$) before adding either the empty pAX142 vector or pAX142 containing CCT construct (10 µg/10 cm dish or 15 µg/15 cm dish, in 1 mg/ml diethylaminoethyl (DEAE)-Dextran in TS buffer) and were incubated for 40 min at 37^{o}C. The positively charged DEAE-Dextran binds to the negatively charged DNA and the complex adsorbs to the negatively charged cellular membranes and is taken up by the cell by endocytosis. The plasmid DNA mixture was aspirated and the cells were incubated in DMEM containing 10 mM Hepes (pH 7.4), 100 µM chloroquine, 5% (v/v) FBS) for 3 h at 37^{o}C. Chloroquine increases the transfection of genes into cells by entering cells and inhibiting lysosomal enzymes thereby preventing degradation of foreign material within lysosomes. The media was then aspirated and the cells were washed with TS buffer. COS-1 cells were shocked for 2 min with TS/20% glycerol (v/v) at room temperature to improve transfection efficiency. The glycerol was aspirated and

the cells were washed with TS buffer. Cells were cultured in fresh media with 5% FBS for 48 h.

Harvesting of transfected COS-1 cells. After 48 h of incubation, the media was aspirated and the dishes with transfected COS-1 cells were washed with warm PBS and incubated for 2 min with PBS/2.5 mM EDTA/2 mM PMSF at 37^{o}C. Cells were then gently dislodged from the plate using a plastic scraper and collected in 50 ml falcon tubes. The dishes were washed again with PBS/2.5 mM EDTA/2 mM PMSF to remove any remaining cells and the cells were collected and centrifuged at 1100 RPM for 3 min. The supernatant was removed by aspiration and the cell pellet was stored at -80^{o}C.

2.2.4. Cell lysis, protein purification, His-tag cleavage and determination of protein concentration

Cell lysis. Hypotonic buffer (20 mM Tris (pH 7.4), 1% Triton, 2 mM DTT) supplemented with protease inhibitors (2.5 µg/ml leupeptin, 2 µg/ml chymostatin, 1 µg/ml antipain, 2 µg/ml pepstatin, 10 µg/ml p-amino-benzadine, 10 µg/ml benzamidine, 2 mM PMSF) was added to the cell pellet. Cells were lysed by sonication on ice for 4 x 20 s using the Fisher Sonic Dismembrator at 30% output. 10X binding buffer (5 M NaCl, 0.15 M imidazole, 0.05 M phosphate buffer, pH 8.0) was added to the cell lysate (1/10) and mixed by gently vortexing. The addition of 10X binding buffer was adapted for Ni-NTA agarose column protein purification of His-CCT from the soluble fraction. The homogenate was separated into supernatant and pellet fractions by centrifugation at 13, 000 RPM for 10 min at 4^{o}C and both fractions were saved.

Purification of His(TEV)-CCT367-T207C. Since His(TEV)-CCT367-T207C was found to be insoluble in cell lysates and quite pure in the pellet fraction, it was prepared from the pellet fraction by denaturation and refolding. The pellet was first resuspended in hypotonic buffer with 1X binding buffer/0.25 mM Triton X-100 (~ 1 mL/15-cm culture dish) and sonicated on ice for 2 x 20 s. Denaturing buffer (10 mM Tris (pH 7.4), 0.5 M NaCl, 0.25 mM Triton X-100, 8 M Urea, 2 mM DTT) supplemented with protease inhibitors (as above) was added and the sample was sonicated on ice for 2 x 20 s. The sample was then centrifuged at 13, 000 RPM for 10 min at 4^{o}C. The denatured protein was slowly refolded by decreasing the concentration of Urea. The supernatant was

dialyzed at 4^{o}C in 3 stages: 1) 5 h against 5 M Urea, 10 mM Tris (pH 7.4), 0.1 M NaCl, 0.25 mM Triton X-100, 2 mM DTT, 2) Overnight against the same buffer but with 2.5 M Urea, and finally 3) 4 h against the same buffer but with 0.5 M Urea. The resultant refolded protein was centrifuged at 13,000 RPM for 10 min at 4^{o}C and was not purified further. The dialyzed protein was aliquoted into small volumes and stored at -80^{o}C.

Cleavage of His-tag. AcTEV^{TM} protease is an enhanced form of the Tobacco Etch Virus (TEV) protease that is used to cleave affinity tags from fusion proteins. This highly site-specific protease recognizes the seven amino acid sequence Glu-Asn-Leu-Tyr-Phe-Gln-Gly and cleaves between Gln and Gly. The His-tag was removed from His(TEV)-CCT367-T207C using 1 unit of AcTEV^{TM} protease per µg of CCT. To determine the incubation time for complete cleavage of the protein, AcTEV^{TM} protease was incubated with protein for 30 min, 1 h and 2 h and aliquots of digested protein were collected after each time point and run on a 10% tricine gel.

The protease was added to the His-tagged CCT and the mixture was rotated at room temperature for 2 h. After incubation NaCl was added to a final concentration of 150 mM and 15 mM of imidazole was also added. AcTEV protease was removed from the cleavage reaction by affinity chromatography using the polyhistidine tag at the N-terminus of the protease. A 1/8 volume of cold 50% Ni-NTA Agarose bead slurry was washed with dialysis buffer (10 mM Tris (pH 7.4), 0.1 M NaCl, 0.25 mM Triton X-100, 0.5 M Urea) and added to the cleavage reaction, and was rotated at room temperature for 30 min. The beads were pelleted by centrifugation at 2000 RPM for 1 min and the supernatant containing the cleaved, untagged CCT was saved. The protein was aliquoted into small volumes and stored at -80^{o}C.

Determination of protein concentration. The concentration of CCT367-T207C was determined using the Nanodrop ND-1000 Spectrophotometer. 2 µl of protein sample was used to read the absorbance at 280 nm.

2.2.5. mBBr fluorescence labelling, protein sample preparation and data collection

mBBr labelling procedure. mBBr (Figure 1.6) is a haloalkyl reagent that readily reacts with thiols to form a stable thiol-ether bond. mBBr was conjugated to the engineered cysteine at residue 207 or 295 of CCT . This small fluorophore is essentially non-fluorescent until it is conjugated. The glutathione conjugate has an absorption/emission maximum of 394/490 nm. A 10 mM stock solution of mBBr was prepared in dimethylsulfoxide (DMSO). The dye was added to the digested protein (to a final concentration of 1 mM) to give approximately 10 moles of reagent for each mole of protein. The same volume of dye was also added to a control sample containing 10 mM Tris (pH 7.4) 150 mM NaCl, 15 mM imidazole, 0.25 mM Triton X-100, 2mM DTT, 0.5 M Urea, but lacking CCT. To determine the incubation time, a sample containing mBBr and CCT367-T207C (10:1) was incubated for 0.5, 1 h and 2 h in the dark. The relative fluorescence unit (RFU) was measured at each time point using the Nanodrop 3300 Fluorospectrometer and it was determined that 0.5 h was sufficient for labeling the protein. After reaction of control and protein sample for 0.5 h at room temperature in the dark to protect the fluorophore, excess thiol-reactive reagent, DTT, was added to quench the reaction. Bimane-DDT conjugates and imidazole were removed by dialyzing for 1 h, 2 h and then overnight against 10 mM Tris, pH 7.4, 150 mM NaCl, 0.25 mM Triton X-100, 0.5 M Urea. The RFU was measured at each time point for both the control sample and sample containing protein and dialysis was considered complete when the RFU value for the control sample decreased and became stable.

mBBr fluorescence: Sample preparation and data collection. Fluorescence emission spectra were acquired with the Nanodrop 3300 Fluorospectrometer. 2 µl of sample was loaded and the dye was excited using the UV LED, which has excitation maxima of 365 nm. The blank for this measurement was the sample lacking protein. The gain was set to be 3.0 for all measurements. The average wavelength of maximum intensity obtained from the emission spectra was 480 nm. The peak RFU values at 480 nm were recorded for each measurement.

Metal titrations: 5 µl samples were prepared with 4.5 µl of the Bimane-labeled CCT and 0 or 1µM – 5 mM Cu^{2+}. These were added from carefully prepared dilutions of

$CuSO_4$. Two readings of each sample were acquired and averaged. Occasionally there was anomalously high fluorescence readings that deviated by > 3 standard deviations from the average value without the anomalous reading. This value was omitted. The RFU values, normalized to the RFU in the absence of metal, were plotted as a function of metal ion concentration.

2.3. Methods for expression, purification, labeling and fluorescence analysis of CCT312 mutants in pET24a

2.3.1. Introduction to the pET-24a(+) expression vector system, general methods for CCT plasmid construction and preparation and QuikChange site-directed mutagenesis.

pET-24a(+). The pET-24a(+) bacterial expression vector allows for expression of target genes under the control of an IPTG-inducible lac promoter, which also controls expression of T7 RNA polymerase, responsible for transcription of the plasmid in the host cell. The T7 polymerase has been engineered into the genome of the BL21(DE3) E. coli cells (see below). The vector also contains an optional C-terminal His-tag sequence, which we did not employ, and a pBR322 origin of replication. The selectable marker is kanamycin. The pET24a-constructs were transformed into Rosetta™ cells, described below.

Rosetta™ cells. Rosetta™ host strains are BL21 derivatives (lack endogenous proteases) that enhance the expression of eukaryotic proteins that contain codons rarely used in *E.coli.* These strains supply tRNAs for the codons AUA, AGG, AGA, CUA, CCC and GGA on a compatible chloramphenicol resistant plasmid, pRARE. The tRNA genes are driven by their native promoters. The pRARE plasmid gives Rosetta cells the special ability to overexpress normally difficult mammalian proteins. Thus Rosetta strains provide for “universal” translation, which is otherwise limited by the codon usage of *E.coli.* Positive transformation is tested with kanamycin and chloramphenicol.

QuikChange site-directed mutagenesis. All site-directed mutagenesis experiments were performed by QuikChange site-directed mutagenesis, a non-PCR

based method of amplification that replicates only the original template DNA using a high fidelity polymerase. It is a rapid method used to introduce site-specific mutations into double-stranded plasmids. A double-stranded DNA vector with an insert of interest is used as a template and two complementary oligonucleotide primers containing the desired mutation are extended during thermo cycling by a high fidelity DNA polymerase. This generates a nicked circular daughter plasmid with the incorporated mutation. An endonuclease, *Dpn*I, is used to digest the methylated, nonmutated parental DNA template strand and specifically select for the daughter DNA containing the desired mutation. The nicked double-stranded daughter DNA is then transformed into XL1-Blue supercompetent cells that repair the nicks.

All QuikChange site-directed mutagenesis experiments were performed using the online manual instructions, with the following exceptions: 1) The oligonucleotide primers were dissolved and diluted to a final concentration of 125 ng/µl in TE buffer prior to usage, 2) *Pfu* DNA polymerase or Phusion DNA polymerase instead of *PfuTurbo* DNA polymerase were used to replicate both plasmid strands, 3) the transcribed daughter DNA with the desired mutation was transformed into either NovaBlue or DH5α competent cells rather than XL1-Blue supercompetent cells, 4) the cycling parameters were slightly varied for each construct (Table A1, Appendix A). The single amino acid substitutions generated by QuikChange site-directed mutagenesis were all confirmed by plasmid DNA sequencing.

Plasmid DNA preparation. Plasmid DNA was isolated from bacterial cells using a QIAprep Spin Miniprep Kit. Cells were lysed under alkaline conditions. The plasmid DNA was purified via retention on silica gel column, while genomic DNA was not retained. The plasmid DNA was eluted in a small volume of Tris-EDTA.

2.3.2. Construction of CCT312 mutants

Construction of pET24a-CCT312-T207C. I assisted Ziwei Ding and Jaeyong Lee with the preparation of the His-tag free, pET24a-CCT312-T207C (Figure 2.2).

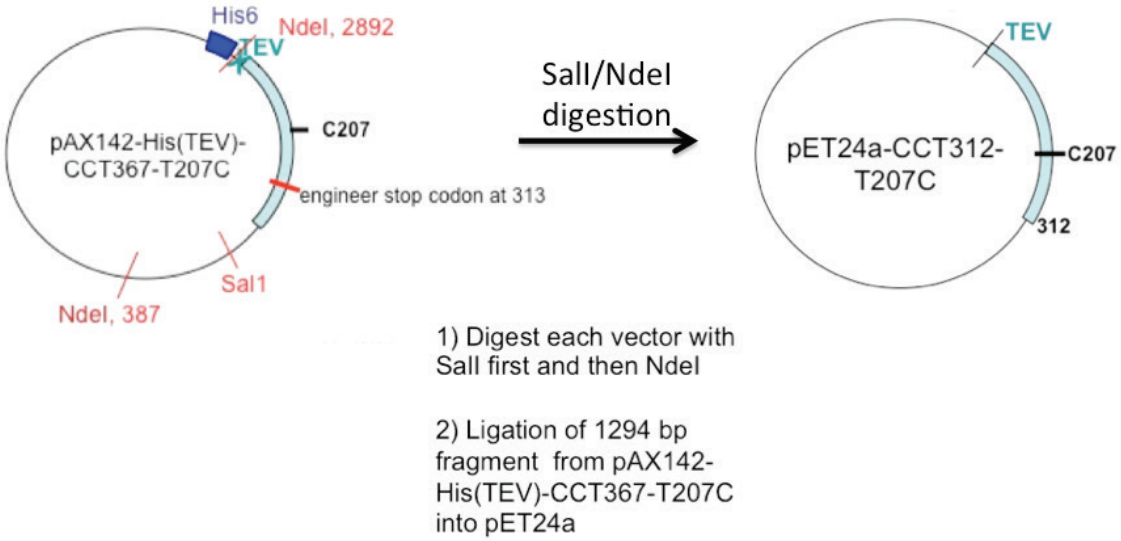

Figure 2.2 Construction of pET24a-CCT312-T207C.
The full-length pAX142-His(TEV)-CCT367-T207C was truncated by QuikChange engineering of a stop codon at 313. The CCT-312-T207C (1294 bp) was then transferred to pET-24a+ using the Nde1 and Sal1 sites, as shown. Since the Nde1 site is down-stream of the His6 in pAX and the Sal1 site is upstream of the His6 in pET24a, the protein is expressed without the His tag.

This construct was transformed into NovaBlue cells. The transformation reaction was incubated on ice for 30 min, heat-shocked for 30 s at 42 ^{o}C and then transferred to ice for 5 min. The cells were plated on LB plates supplemented with kanamycin and grown overnight at 37^{o}C. Colonies were picked, cultured and plasmids prepared for sequencing.

pET24a-CCT312-H89S-T207C was constructed using pET24a-CCT312-T207C as the template along with two complementary oligonucleotide primers (See Appendix B for oligonucleotide primer sequence) and **pET24a-CCT312-H89A-T207C** was constructed using pET24a-CCT312-H89S-T207C as the template along with two complementary oligonucleotide primers (See Appendix B for oligonucleotide primer sequences). **pET24a-CCT312-P295C** was prepared by Ziwei Ding. The cysteine residue at site 207 in pET24a-CCT312-T207C was reverted back to a threonine using QuikChange site-directed mutagenesis. In the following step this cysteine-free construct was used as a template along with two complementary oligonucleotide primers (See Appendix B for oligonucleotide primer sequences) to create pET24a-CCT312-P295C.

2.3.3. Expression, purification methods and determination of protein concentration for CCT312 constructs in pET24a.

Expression of protein via IPTG induction. Starter cultures (5 ml) were prepared by inoculation of LB media with a single colony of Rosetta cells harbouring the pET-24a(+)-CCT plasmid and were incubated at 37^{o}C overnight with shaking. The next day the starter culture was transferred to 100 or 200 ml of LB media (Table C1, see Appendix C) supplemented with kanamycin and chloramphenicol. The cultures were incubated for 4 h at 37^{o}C with shaking and were grown to an optical density (Abs_{600nm}) of 0.6-0.8. Overexpression was induced with 1mM of Isopropyl β-D-1-thiogalactopyranoside (IPTG) and the cultures were incubated at 37^{o}C for 3 h. After the induction period, cells were harvested by centrifugation at 4000 x g for 15 min. The supernatant was decanted and the cell pellet was frozen at -80 C.

Cell lysis. Lysis buffer composed of 10 mM Tris (pH 7.4), 150 mM NaCl, 2mM DTT, 0.1 mg/ml lysozyme and 1% Triton was added to the cell pellet and the cells were lysed by sonication on ice for 3 x 15 s. The volume of lysis buffer used is specified in Table C1 (Appendix C). The homogenate was separated into supernatant and pellet fractions by centrifugation at 13, 000 RPM for 10 min at 4^{o}C. Small aliquots of both fractions were collected and electrophoresed using 10% tricine gels to determine if the protein was present in the supernatant or pellet.

Preparation and extraction of insoluble proteins (inclusion bodies) from *E.coli.* The pellet fractions, containing inclusion body proteins, were washed thrice to remove contaminants. The volumes of washing buffer (10 mM Tris (pH 7.4), 150 mM NaCl, 1 mM EDTA, 2 mM DTT, 1% Triton) used to resuspend the pellets are specified in Table C1 (Appendix C). The samples were sonicated on ice for 3 X 15 s, and separated into insoluble pellet and supernatant fractions by centrifugation at 13, 000 RPM for 15 min at 4^{o}C and the pellet fraction was saved.

***In vitro* denaturation and slow refolding of protein.** The washed inclusion body pellets were resuspended and incubated in a strong denaturant (6 M GuHCl), using the volumes specified in Table C1 (see Appendix C). Remaining particulates were removed by centrifugation at 13, 000 RPM for 15 min at 4^{o}C. The solubilized, denatured

protein was slowly refolded by decreasing the concentration of denaturant using dialysis at 4°C in 3 stages: 1) Overnight against 3 M GuHCl, 10 mM Tris (pH 7.4), 150 mM NaCl, 2 mM DTT, 2) During the day against the same buffer but with 1.5 M GuHCl and finally 3) Overnight against the same buffer but with no GuHCl. After dialysis, the samples were spun at 13,000 RPM for 15 min at 4°C and the supernatant was saved for purification.

Protein purification. The refolded CCT samples were purified using a SP-Sepharose cation exchange column containing 1.5 ml of beads. The supernatant fraction was loaded onto 1.5 mL of beads in a column equilibrated with EQ buffer (10 mM Tris (pH 7.4), 150 mM NaCl, 2 mM DTT) and the flow-through was collected. The beads were then washed again with EQ buffer. The bound protein was eluted from the column with EQ buffer containing 200 mM NaCl, 300 mM NaCl, 400 mM NaCl and 500 mM NaCl (in that order). Elution fractions (volumes specified in Table C1, Appendix C) were electrophoresed using 10% tricine gels to determine which elution fraction contained the highest concentration of protein.

Determination of protein concentration. The concentrations of the purified proteins were determined using the Nanodrop ND-1000 Spectrophotometer. 2 µl of sample was used to read the absorbance at 280 nm. The extinction coefficients were computed by importing the sequence into the ProtParam tool on the ExPASy Website.

2.3.4. mBBr labelling, protein sample preparation and data collection

mBBr labeling procedure. The protocol was as described in section 2.2.5 with the following modifications: A 29 mM stock solution of mBBr was prepared in DMSO immediately prior to use. A 10-fold molar excess of DTT was added to purified protein to reduce disulfide bonds and this mixture was incubated at room temperature for 30 min with rotation. The sample was then dialyzed for 1 h against EQ buffer containing 300 mM NaCl to remove the excess DTT prior to introduction of the reactive dye. The control sample was composed of EQ buffer (with 300 mM NaCl) and no protein. After labeling, excess DTT and bimane-DDT conjugates were removed by dialyzing for 5 h against EQ buffer with 300 mM NaCl (with a buffer change every 2 h). Labeling was confirmed by visualization of fluorescent bands on a 10% tricine gel (containing the bimane-labeled

CCT) using the Continuum opo (Panther) nanosecond pulsed laser with a violet laser irradiation. When the gel was irradiated at 410 nm, the band associated with the unreacted CCT appeared purple, whereas the labeled-protein band appeared blue (fluorescence emission is red-shifted). The mBBr-labeled proteins were stored in the dark at -80^{o}C.

mBBr fluorescence: Sample preparation and data collection. The protocol was as described in section 2.2.5, with the following modifications: Bimane-labeled protein was mixed with increasing concentrations of Cu^{2+} and diluted in 10 mM Tris (pH 7.4) and 0.1 M NaCl. The final protein concentration was 0.5 µM. Samples (400 µl) were placed in a 10 mm path-length quartz cuvette and spectra were obtained using the Varian Cary Spectrofluorometer with excitation set at 394 nm and an emission scan from 420-650 nm. Both the excitation and emission slits were set to 10 nm and the PMT (photomultiplier tubes) voltage was kept constant for each experiment. Spectra were saved and the peak emission intensity was acquired manually. The average wavelength of maximum intensity was at ~470 nm. After subtracting the associated value for the control spectra containing no CCT, the adjusted intensity values for the titration set were transferred to an Excel spreadsheet. Data were plotted as (Fmetal/F) as a function of metal ion concentration for each protein, where F = fluorescence obtained in the absence of metal.

2.3.5. Western Blotting

Proteins electrophoresed on a 10% SDS gel were transferred to a PVDF membrane using a transfer blot apparatus (2 mAmp/cm^2 gel surface area) for 1 h in transfer buffer (39 mM Glycine, 48 mM Tris, 0.0375% SDS). The membrane was blocked in Blotto (TBS containing 1% Tween-20, 10% milk powder) by incubating for 1 h at room temperature, washed with 1% Tween-20/TBS solution, followed by a 2 h room temperature incubation with primary antibody (diluted 1/600 in Blotto), anti-N directed against the first 15 residues of rat CCT. The membrane was washed with 1% Tween-20/TBS solution and incubated for 1 h at room temperature with the secondary antibody, GAR-HRP (diluted 1/2000 in Blotto). The membrane was then washed as before. When anti-M (1/2000 dilution) (directed against residues 256-288) instead of anti-N was used

as the primary antibody, the membrane was blocked in Blotto composed of TBS 0.2% Tween-20 and 6% milk powder. The membrane was washed with 0.2% Tween-20/TBS solution. The antibody-bound protein was visualized using a Fuji ImageReader LAS 4000.

2.3.6. CCT enzyme activity analysis

The CCT activity assay measures the amount of labeled CDP-choline produced by CCT using [^{3}H]-phosphocholine as a substrate. The CCT activity assays were carried out as described in (Taneva, Dennis et al. 2008) The assays were carried out in the absence or presence of egg PC/egg PG (1/1, mol/mol) sonicated vesicles. The lipid concentration in these assays was 0.1 mM.

Chapter 3. Results

3.1. Overview of research work

My thesis work involved optimizing a fluorescence method called transition metal ion FRET (tmFRET) that uses energy transfer between a small fluorophore and a transition metal ion bound to a di-histidine motif to study intra-molecular movements in proteins. My specific goal was to probe the interaction between the catalytic and membrane-binding domain of CCT using this tmFRET approach. The first step was to assess the efficacy of a native di-histidine motif in the active site as a metal ion-binding site and FRET acceptor. If effective, this would preclude the need to engineer a di-histidine motif, and would eliminate the possibility of unintended structural perturbation. The FRET donor, and site of cysteine engineering and bimane conjugation, was initially T207C in helix αE. Helix αE is the segment extending from the base of the active site (Figure 1.3, Chapter 1). This single cysteine variant had previously been characterized by Harris Huang (Huang, Taneva et al. 2013) and was found to have no effect on CCT activity. In the solved structure of the CCT catalytic domain (Lee, Johnson et al. 2009), H89 and H92 are respectively 12 Å and 14 Å away from T207 (Figure 3.1), a distance amenable to analysis by tmFRET (Taraska, Puljung et al. 2009). Thus the C207 donor site was chosen as a proof-of-principle for the use of the native di-histidine as a FRET acceptor site.

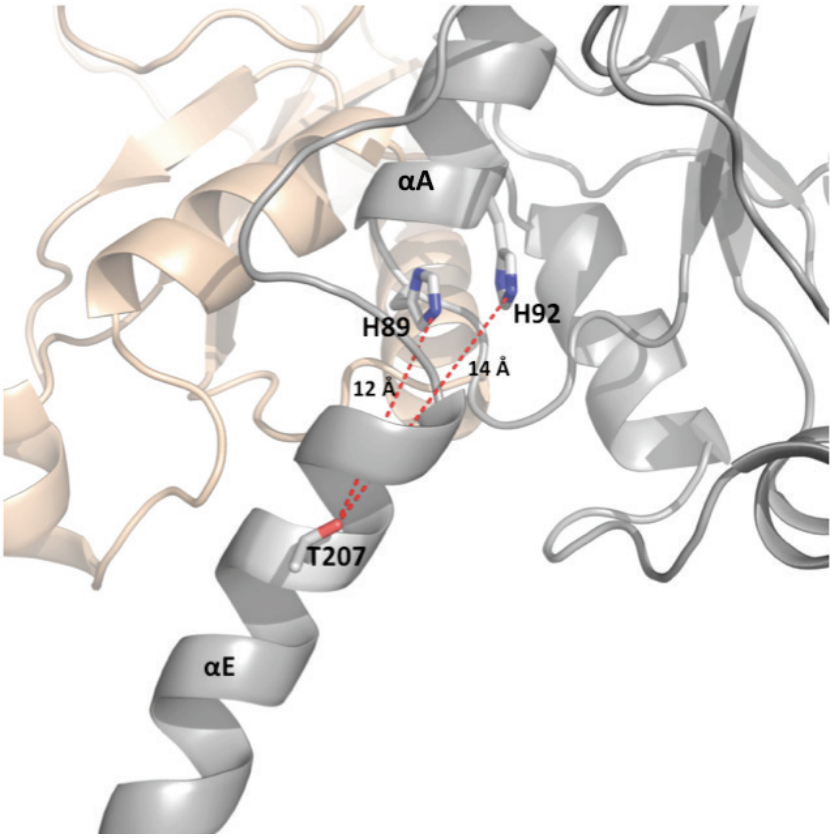

Figure 3.1 Distance between histidines in ^{89}HSGH^{92} and T207.
H89 and H92 are respectively 12 Å and 14 Å away from T207. H89 and H92 are located in the conserved HSGH motif in helix αA and T207 in helix αE of CCT. This image was generated in PyMOL using PDB: 4MVC.

I worked with rat CCTα variants containing a single engineered cysteine (Figure 3.2). In my initial experiments, I utilized a full-length His-tagged CCT construct, CCT367-T207C. In the first part of this chapter, I discuss the results and describe the problems I encountered while working with this particular construct and explain why I later switched to working with His-tag free CCT312 mutants. CCT312 constructs containing a substitution of the histidine residue at position 89 to a serine or alanine (CCT312-H89S-T207C and CCT312-H89A-T207C) were prepared in an attempt to disrupt the metal binding site. I later utilized a CCT312 construct with a single cysteine substitution at position 295 for bimane conjugation at the end of the AI motif, in domain M, to probe the interactions between domains M and C in the presence or absence of activating lipids.

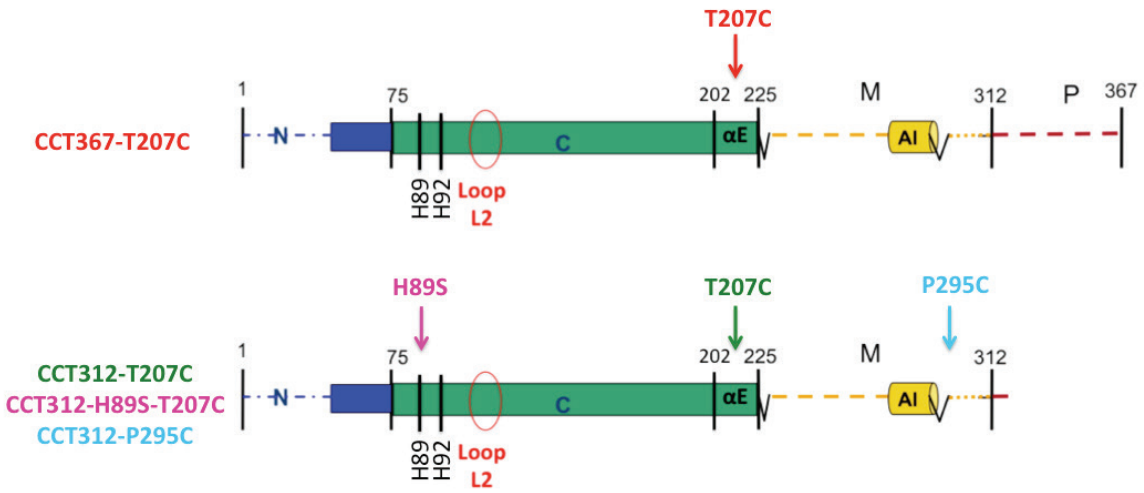

Figure 3.2 The CCTα variants used in experiments.
CCTα variants containing a single engineered cysteine for bimane modification in helix αE (C207) or at the end of the AI motif (C295). A construct containing an H89S change is also shown.

3.2. Expression and purification of His(TEV)-CCT367-T207C

The His-tagged full-length CCT367-T207C construct was expressed in COS-1 cells for 48 h. The 44 kDa CCT was found almost exclusively in the insoluble 13,000 g pellet, indicating that this construct is aggregation-prone (Figure 3.3).

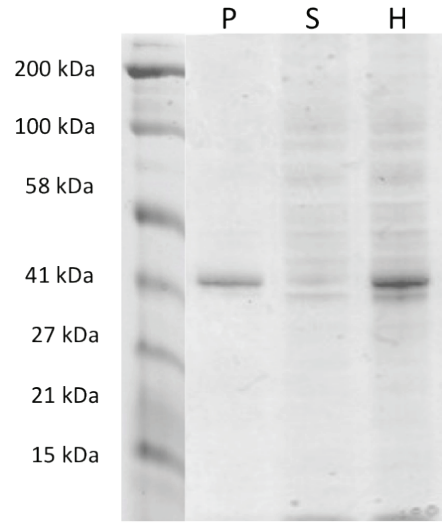

Figure 3.3 Expression of His(TEV)-CCT367-T207C in pellet fraction of COS-1 cells. Cell lysates were separated into soluble and insoluble pellet fractions as described in the methods section. The 10% tricine gel shows the pellet (P), supernatant (S) and homogenate (H) fractions. Proportional aliquots of each fraction were loaded on a 10% tricine gel, which was stained with Coomasie Blue.

To recover the protein, the insoluble pellet was first re-suspended in buffer containing a chaotropic agent (urea) that denatures the protein. The solubilized protein was then refolded by slow removal of the denaturant during dialysis. Figure 3.4 shows that about 50% of the protein was recovered after dialysis in the supernatant but some was also lost to the pellet. The presence of a single band on the gel lane containing the supernatant fraction indicated that the final refolded protein was relatively pure. Therefore, no additional techniques were employed to further purify the protein.

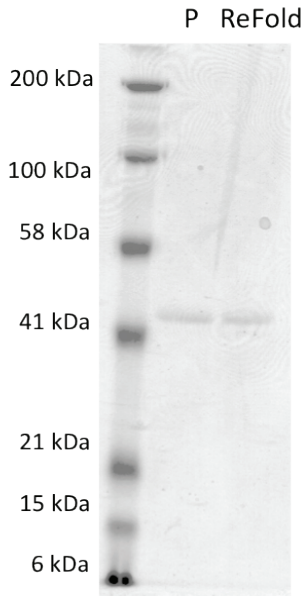

Figure 3.4 Renaturation of Urea denatured His(TEV)-CCT367-T207C.
The insoluble His(TEV)-CCT367-T207C protein was denatured in buffer containing 8 M urea and then refolded by dialysis as described in the methods section. The solubility of the final dialyzed CCT was assessed by centrifugation at 13,000 rpm. The 10% tricine gel shows the pellet (P) fraction and supernatant containing refolded protein (ReFold). Proportional aliquots of each fraction were loaded on each lane. Gel was stained with Coomasie Blue.

3.3. Cleavage of His-tag with AcTEV protease

The poly (His) tag in His(TEV)-CCT367-T207C was removed to prevent transition metal ions from associating with these histidines during FRET analyses. The histidine tag was excised using the AcTEV protease site between the tag and start of the CCT sequence. Figure 3.5 shows that complete cleavage of the protein was achieved after 2 h of incubation as indicated by the small band shift on the gel, whereas only partial cleavage was attained after 30 min. These results also confirmed that AcTEV protease cleaved specifically at the linker site and not anywhere within the CCTα sequence, as there was only one cleavage product. The molecular weight of the cleaved protein is approximately 41 kDa.

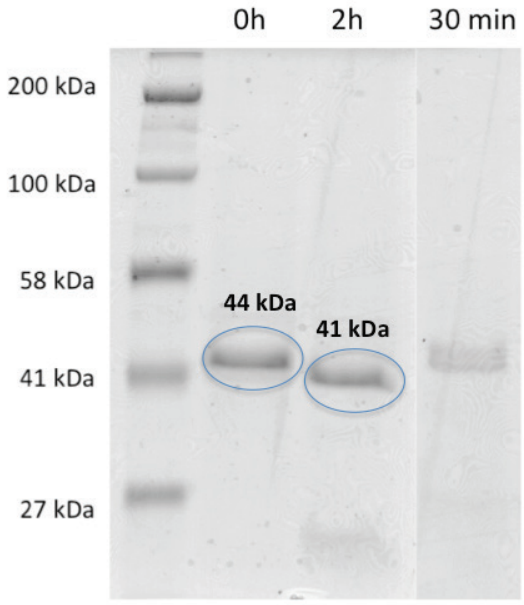

Figure 3.5 AcTEV cleavage of His-tag.
The 10% tricine gel shows CCT367-T207C after 0 h, 2 h and 30 min of AcTEV cleavage of His-tag. The faster migration of the protein band after the addition of protease indicates that the His-tag is removed. The molecular weight of the protein is 44 kDa and after 2 h of AcTEV cleavage is approximately 41 kDa. Proportional aliquots of each fraction were loaded on each lane.

Since the AcTEV protease has a poly-histidine tag at the N-terminus, it can be easily removed from the cleavage reaction by adding Ni-NTA agarose beads. Figure 3.6 shows three supernatant fractions collected after centrifugation and the Ni-NTA agarose beads. Some cleaved, untagged CCT was recovered in the supernatant after the first centrifugation step. Subsequent washes did not yield any protein (lanes 4 and 5); instead most of the cleaved protein was firmly bound to the Ni-NTA agarose beads.

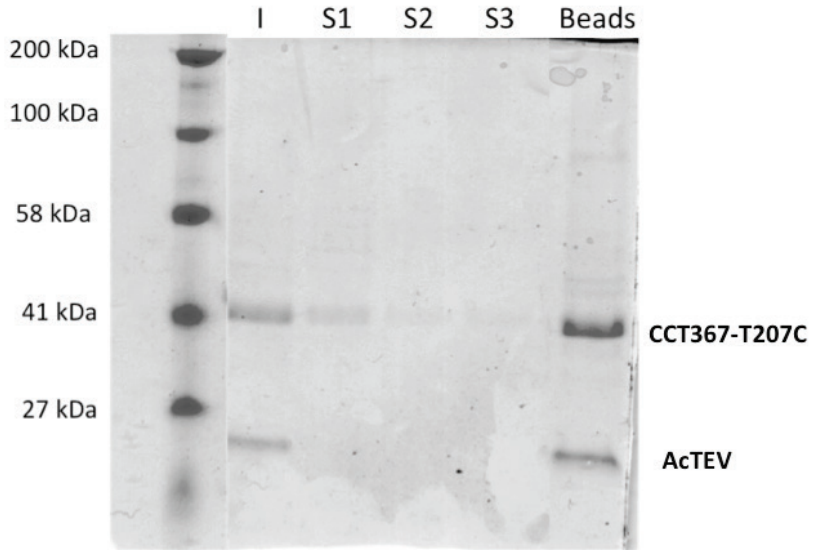

Figure 3.6 Removal of cleaved His-tags and AcTEV protease.
His-AcTEV protease and cleaved His-tags were removed from the cleavage reaction by affinity chromatography, as described in the methods section. The 10% tricine gel shows the initial cleaved protein (I), supernatants collected after the beads were pelleted 3x (S1, S2 and S3) and the Ni-NTA Agarose beads (Beads). Proportional aliquots of each fraction were loaded on each lane.

3.4. Fluorescent labeling of CCT367-T207C with mBBr

Purified CCT367-T207C was conjugated with mBBr for various times and an increase in fluorescence at 480 nm was taken as an indication of successful conjugation to C207, as the unreacted mBBr is internally quenched. Conjugation of the protein's cysteine sulfhydryl results in the loss of the quenching bromo group. Figure 3.7 shows that reaction times of 30 min, 1 h or 2 h yield similar RFU values (~ 13,000). Based on this, I chose the shortest duration (30 min) for labeling CCT367-T207C.

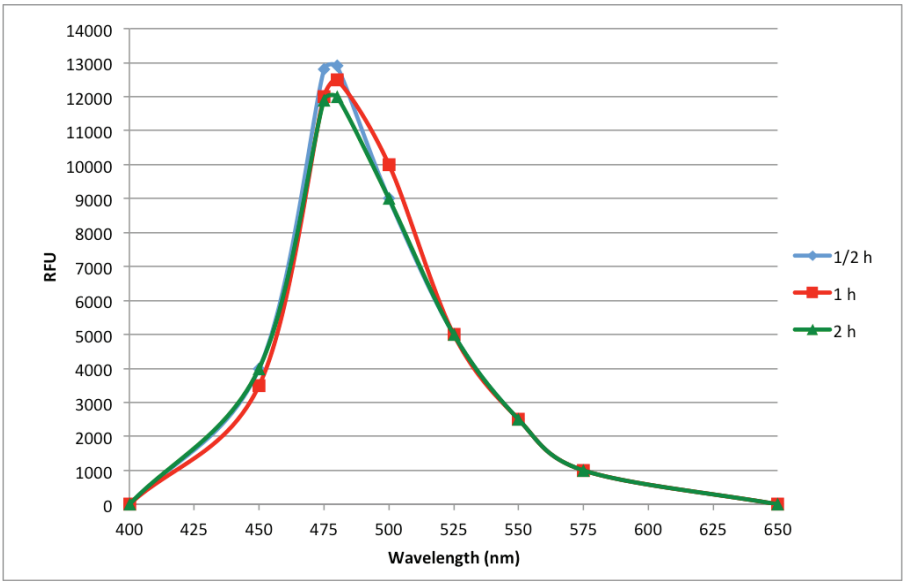

Figure 3.7 Time-course of fluorescent labeling.
CCT367-T207C was labeled with mBBr for the indicated times in the dark. The relative fluorescence units (RFU) were reported against wavelength using the Nanodrop 3300 fluorospectrometer. The dye conjugated to CCT367-T207C has an absorption/emission max of 394/480 nm.

Upon completion of the reaction, the excess thiol-reactive mBBr was removed by dialysis to ensure that there were no reactive-species present in the final labeled protein sample. DTT was initially added to the protein to reduce disulfide bonds and make sulfhydryl groups available for conjugation to the dye. I observed that when excess DTT was present in the reaction mixture, the fluorescence was enhanced (data not shown), likely because mBBr can react with the two sulfhydryl groups on DTT in addition to interacting with CCT367-T207C. Therefore, excess mBBr or bimane-DTT conjugates were removed by dialysis before proceeding to conducting tmFRET experiments.

3.5. tmFRET analyses on mBBr-modified CCT367-T207C

To explore close-range FRET between bimane and Cu^{2+}, fluorescence-quenching experiments were performed on bimane-labeled CCT367-T207C in solution. I added increasing concentrations of Cu^{2+} ranging from 1 μM to 5 mM to a constant concentration of bimane-modified protein and monitored the decrease in bimane's fluorescence emission. Fluorescence from the protein in the presence of metal (F_{metal})

was normalized to the initial fluorescence value without metal (F). The amount of quenching (F_{metal}/F) at the peak (480 nm) of the spectrum was then plotted as a function of Cu^{2+} concentration (Figure 3.8, blue diamonds). A decrease in fluorescence was observed in the range of 10^{-5} to 10^{-3} M Cu^{2+}.

Previous findings (Taraska, Puljung et al. 2009) have suggested that there are two components to fluorescence quenching in tmFRET: a) high affinity quenching caused by the binding of metal ions to engineered dihistidine motifs and b) low affinity quenching caused by metal ions in solution. FRET-based quenching typically occurs at very low nanomolar or micromolar concentrations of Cu^{2+}, whereas collisional quenching occurs close to and above 10^{-5} M of Cu^{2+} (Yu, Wu et al. 2013). To assess if the quenching I observed was strictly collisional, FRET-based or a combination of the two, I analyzed quench behavior for bimane-labeled protein by: a) saturating the protein with CDP-choline (10 mM) and b) lowering the pH of the fluorescence buffer (pH 6). The first experiment was predicated on the knowledge that CDP-choline binds to the ^{89}HSGH^{92} site. The solved structure of CCT with bound CDP-choline revealed that the ^{89}HSGH^{92} site participates in product binding (Lee, Johnson et al. 2009). I predicted that the bound CDP-choline would prevent Cu^{2+} from accessing the histidines, thereby preventing quenching of the fluorophore. However, based on the results of figure 3.8, it appears that the quenching effect is greater in the presence of CDP-choline (green triangles). The second experiment was predicated on the knowledge that at a pH below its pKa, the protonated form of histidine dominates and the histidines lose their Cu^{2+} ion chelating ability. Therefore under acidic conditions there should be no quenching of bimane fluorescence. Interestingly, the results showed that low pH does not prevent quenching of bimane (Figure 3.8, red circles). The three quench curves in figure 3.8 follow the same trend and notably, robust quenching occurs between 10^{-5} and 10^{-3} M of Cu^{2+}. Altogether, these results seem to suggest that the ^{89}HSGH^{92} site is not effective as a high affinity Cu^{2+} binding site. Rather, these data could strictly reflect collisional quenching.

However, there are alternative explanations that could account for the quenching obtained at pH 6 and in the presence of CDP-choline other than strictly collisional (See

Chapter 4). Thus I later tried an additional probe of the utility of the HSGH site by mutation of His89 (See section 3.10). This mutation should destroy the Cu^{2+} binding site.

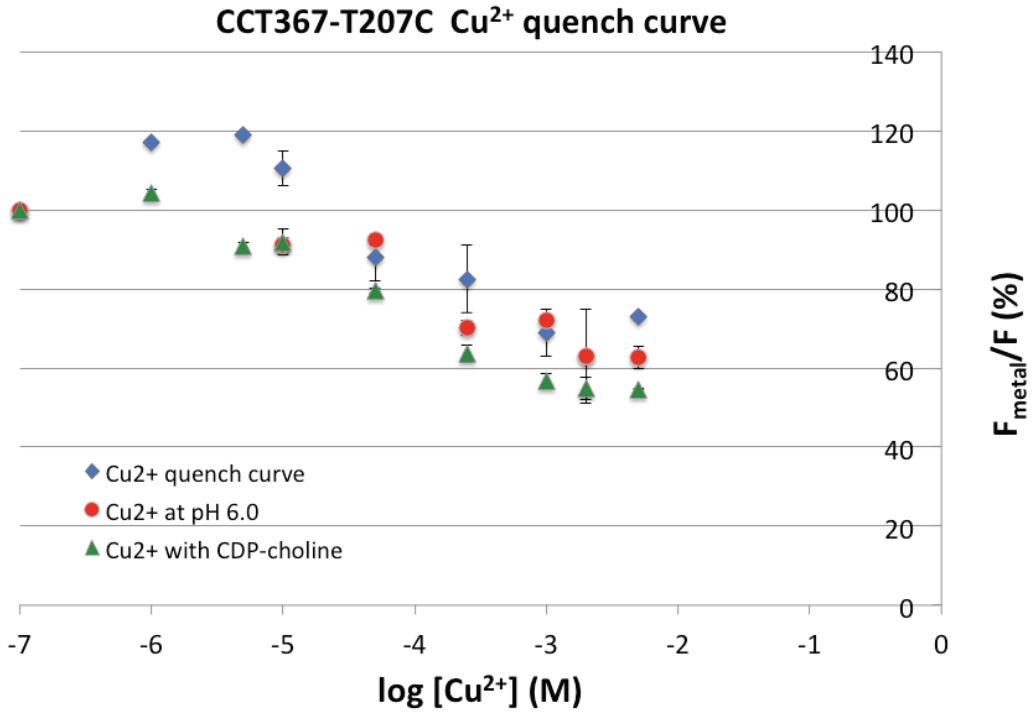

Figure 3.8 Plots of Cu^{2+} dependent quenching of CCT367-T207C.
Average Cu^{2+} quenching of mBBr-reacted CCT367-T207C's at pH 7.4 (blue diamonds), at pH 6.0 (red circles) and in the presence of 10 mM CDP-choline, pH 7.4 (green triangles). The value, -7, on the X-axis denotes 0 µM (no Cu^{2+}).The results are averages of 2 replicates +/- standard error.

3.6. Challenges facing the use of pAX142-His(TEV)-CCT367-T207C

His(TEV)-CCT367-T207C was not used going forward due to some of the recurring challenges I faced while conducting experiments. The preparation of this construct suffered from large losses in protein at the refolding step (Figure 3.4) and the His-tag removal step (Figure 3.6). Further protein losses occurred during subsequent dialysis procedures where some of the protein stuck to the dialysis tubing. I was finally left with very little protein to conduct tmFRET experiments. To overcome these challenges, I switched to working with a His-tag free CCT312 construct for which expression and purification protocols had previously been developed. This would eliminate the large losses due to non-specific absorption to nickel-agarose. Moreover, it

was expected that the expression levels would be enhanced using the bacterial *vs* COS expression system. This construct encodes residues 1-312 and is missing only the disordered phosphorylation region, which affects neither the folding of the rest of the protein nor catalytic activity (Dennis, Taneva et al. 2011).

3.7. Expression and *in vitro* denaturation and refolding of CCT312 mutants

The following CCT312 mutants were effectively expressed in Rosetta strain of *E.coli*: CCT312-T207C, CCT312-H89S-T207C and CCT312-P295C. Overexpression of these mutants was observed after 3 h of IPTG induction at 30^{o}C (Figure 3.9 and 3.10). The expression of the H89A mutant was poor (data not shown). Thus I did not work with this construct going forward.

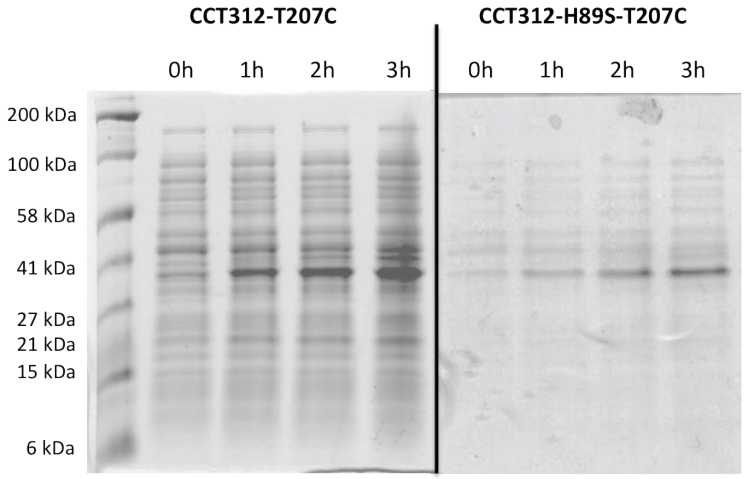

Figure 3.9 Overexpression of CCT312-T207C and CCT312-H89S-T207C.
E. coli Rosetta cells harboring the indicated pET-24a-CCT constructs were induced for 3 h with 1 mM IPTG at 37^{o}C. The molecular weight of the protein is 37 kDa. Proportional aliquots of lysates were separated on a 10 % tricine gel, stained with Coomassie Blue.

High-level expression of the mutants in *E.coli,* lead to the formation of aggregated proteins (inclusion bodies). All three proteins were expressed predominantly in the insoluble form (Figure 3.10).

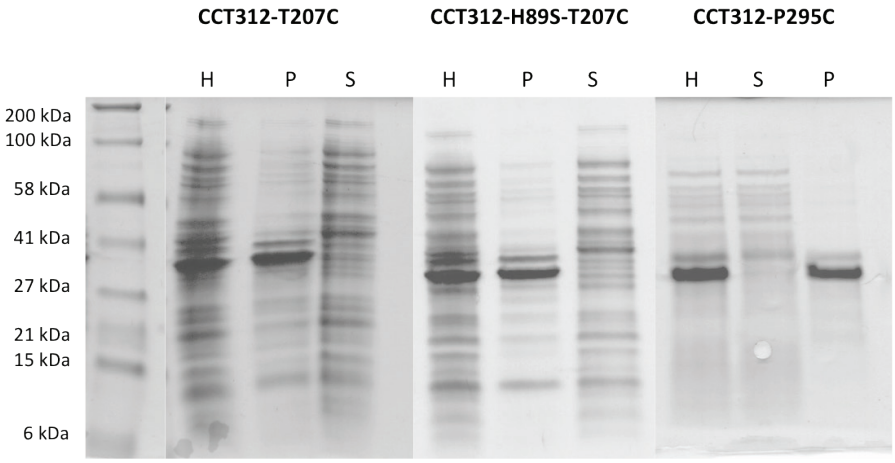

Figure 3.10 Expression of CCT-312 variants in the pellet (IB) fraction of Rosetta cells.

Cells harboring the indicated pET-24a-CCT constructs were induced for 3 h with 1 mM IPTG at 37^{o}C. The 10% tricine gels show the homogenate (H), supernatant (S) and pellet (P) fractions of the protein. Proportional aliquots of each fraction were loaded on each lane of 10% tricine gels, which were stained with Coomasie Blue.

Since the CCT312 mutants were found to be insoluble in cell lysates, they were denatured and refolded *in vitro*. Figure 3.11 shows that some of the protein was lost to inclusion body washes. Most of the protein remained soluble (ReFold fraction in figure 3.11), however some unfolded protein was lost to the pellet.

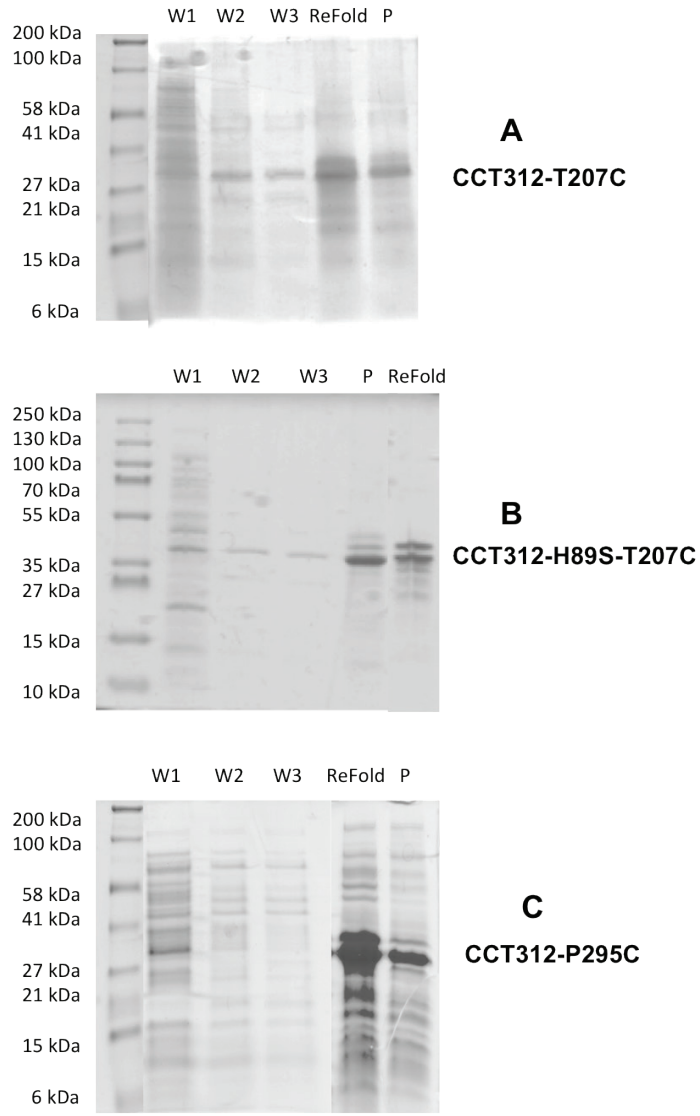

Figure 3.11 Renaturation of Guanidine Hydrochloride denatured CCTs.
The inclusion body pellets were resuspended in wash buffer 3x and the proteins were denatured in 6M GuHCl and refolded by dialysis as described in the methods section. The 10% tricine gels show the supernatant fractions after each wash (W1, W2 and W3) and the refolded protein (ReFold), which remains in the supernatant, and pellet (P) fraction after dialysis. Proportional aliquots of each fraction were loaded on each lane.

3.8. Ion exchange purification of CCT312 mutants

The refolded soluble CCT312 variants were further purified using a SP-Sepharose ion exchange purification column (Lee, Taneva et al. 2014). Most of the protein was recovered in the 300-400 mM NaCl elution fractions (Figure 3.12).

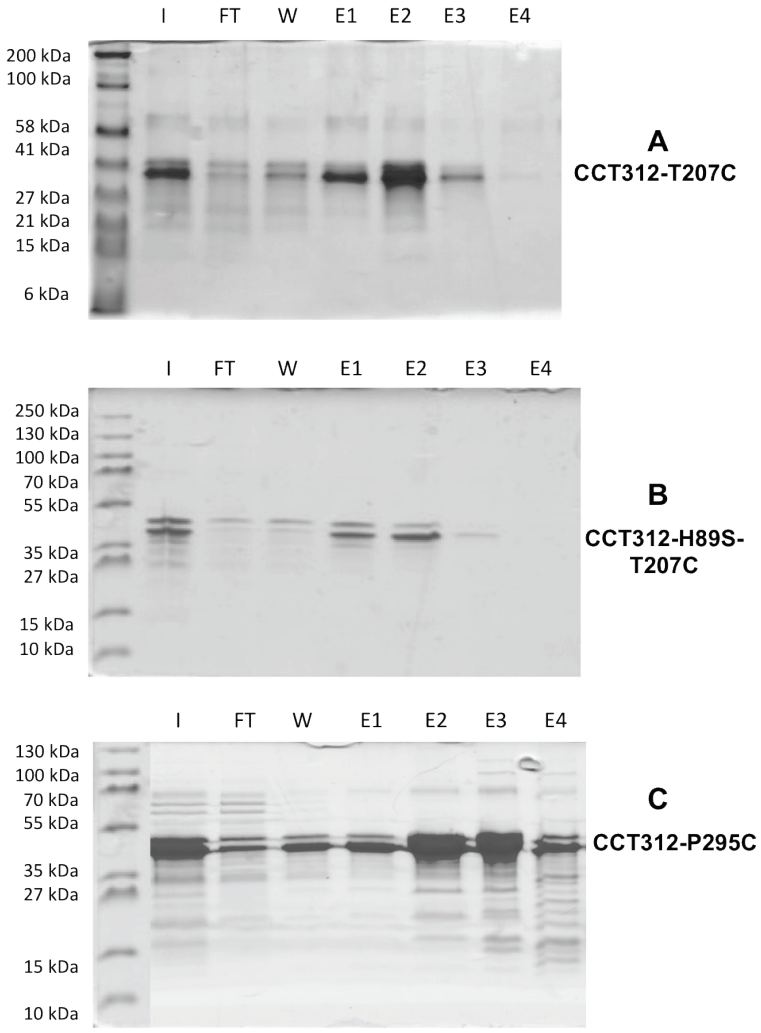

Figure 3.12 Purification of CCT312 mutants.
The refolded proteins were purified using a SP-Sepharose ion-exchange purification column as described in the methods section. The 10% tricine gels show the input (I), flow-through (FT), wash (W) and elution fractions E1-E4, which represent the protein eluted in 200, 300, 400, and 500 mM NaCl. Proportional aliquots of each fraction were loaded on each lane. The E2 fraction was generally used for conjugation with mBBr.

3.9. Western blot analysis of CCT312-T207C

CCT312 variants purified from the *E. coli* system appeared as 2 bands when run on a 10% tricine gel (Figure 3.13). To confirm that both bands were CCT-derived I conducted a western blot on CCT312-T207C. The primary antibodies anti-N or anti-M were used for detection of the target protein. Anti-N is directed against the first 15 residues of CCT and anti-M is directed against residues 256-288. Figure 3.13 shows that

both the top and bottom bands were detected using anti-N and anti-M, implying that both are CCT-derived. It is possible that in the pET24a vector, translation starts at a methionine eleven codons 5' of the CCT start codon (minor initiation site) in addition to the major translation start at the authentic CCT initiator methionine. This would result in the addition of ~1500 Da to the mass of the expressed CCT, and explain the upper band.This would apply to pET24a constructs only.

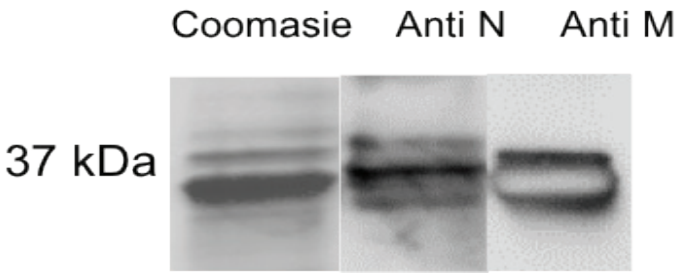

Figure 3.13 Western blot analysis of CCT312-T207C.
CCT312-T207C shows up as two bands on a 10% tricine gel. Both the top and bottom bands were detected using Anti-N and Anti-M antibodies indicating that both bands belong to the protein. The signal from the secondary antibody, GAR-HRP, was visualized with Fuji ImageReader LAS 4000.

3.10. tmFRET analyses on mBBr-modified CCT312 mutants

3.10.1. tmFRET analyses of CCT312-T207C and CCT312-H89S-T207C

As mentioned in section 3.5, mutation of the first histidine of the ^{89}HSGH^{92} site to serine would provide a strong test of the utility of this site as a FRET acceptor. Previous analyses have suggested that a single histidine does not provide a strong binding site for the metal ion (Taraska, Puljung et al. 2009). Therefore, I expected to observe very minimal FRET except only at high concentrations of Cu^{2+} (> 10^{-4} M). On the contrary figure 3.14B shows that the bimane-modified protein with the single histidine exhibited substantial quenching starting at 10^{-5} M of Cu^{2+}, similar to that observed for CCT312-T207C (Figure 3.14A). These data were transformed into the quench curves shown in figure 3.15. Figure 3.15 shows that there was little difference between the construct (CCT312-T207C) with the native di-histidine motif intact (Figure 3.15A) and the construct

(CCT312-H89S-T207C) with a single histidine (Figure 3.15B). These results suggested that the native di-histidine motif was not an effective metal binding site.

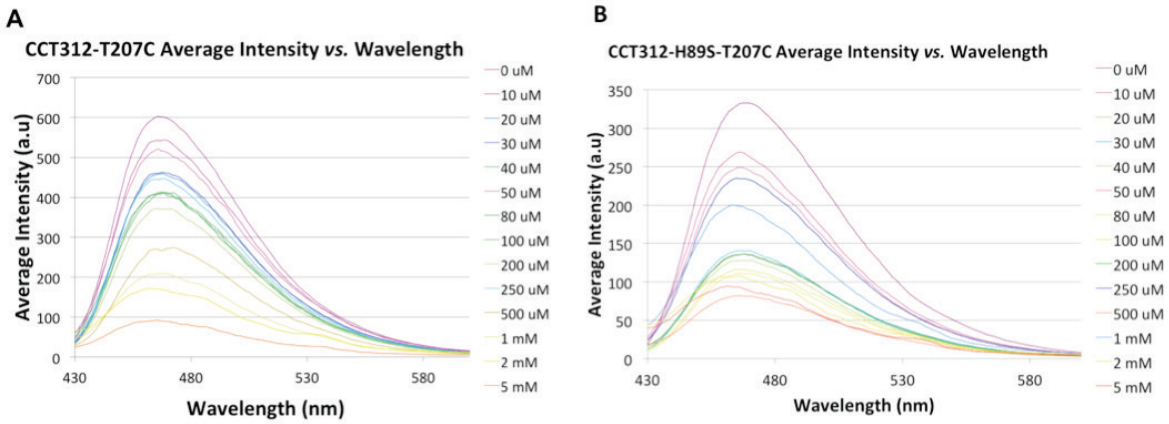

Figure 3.14 Effect of Cu^{2+} on the spectra of bimane-labeled CCT312-T207C and CCT312-H89S-T207C

Spectra of the indicated mBBr-reacted CCT312 mutants at increasing concentrations of Cu^{2+} ranging from 0 µM – 5 mM.The dye conjugated to the CCT312 mutants has an absorption/emission max of 394/470 nm. Bimane's emission decreases upon titration of metal.

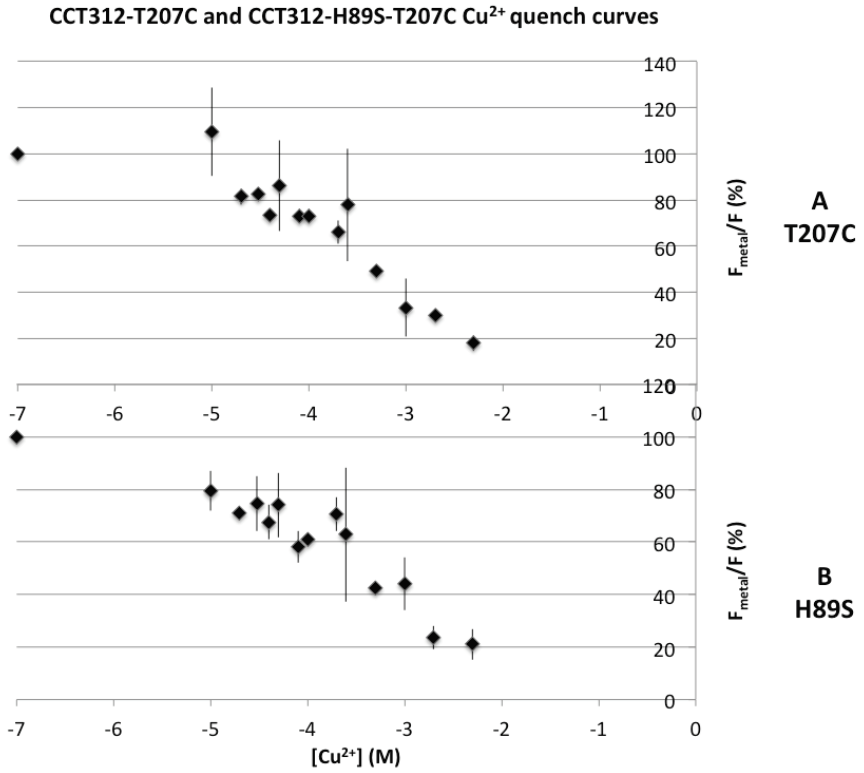

Figure 3.15 Cu^{2+}quenching curves for CCT312-T207C and CCT312-H89S-T207C.

Average Cu^{2+} quenching of mBBr-reacted CCT312 mutants (A) CCT312-T207C and (B) CCT312-H89S-T207C. The value, -7, on the X-axis denotes 0 µM (no Cu^{2+}). The results are averages of 2 replicates +/- standard error.

3.10.2. Probing tmFRET between the AI motif and active site di-histidine

We considered that the conjugation of mBBr to the site selected in helix αE (T207C) might have been an impedance to effective FRET with the native ^{89}HSGH^{92} acceptor site, as the pathway between C207 and the di-histidines is not barrier-free. To further probe the efficacy of the ^{89}HSGH^{92} site, the mBBr conjugation site was changed from C207 to C295 at the end of the AI motif. This would probe interactions between domains M and C. The path between C295 and the di-histidines is barrier-free. The histidines in the HSGH motif and P295 are separated by a distance of 13.5 Å (Figure 3.16).

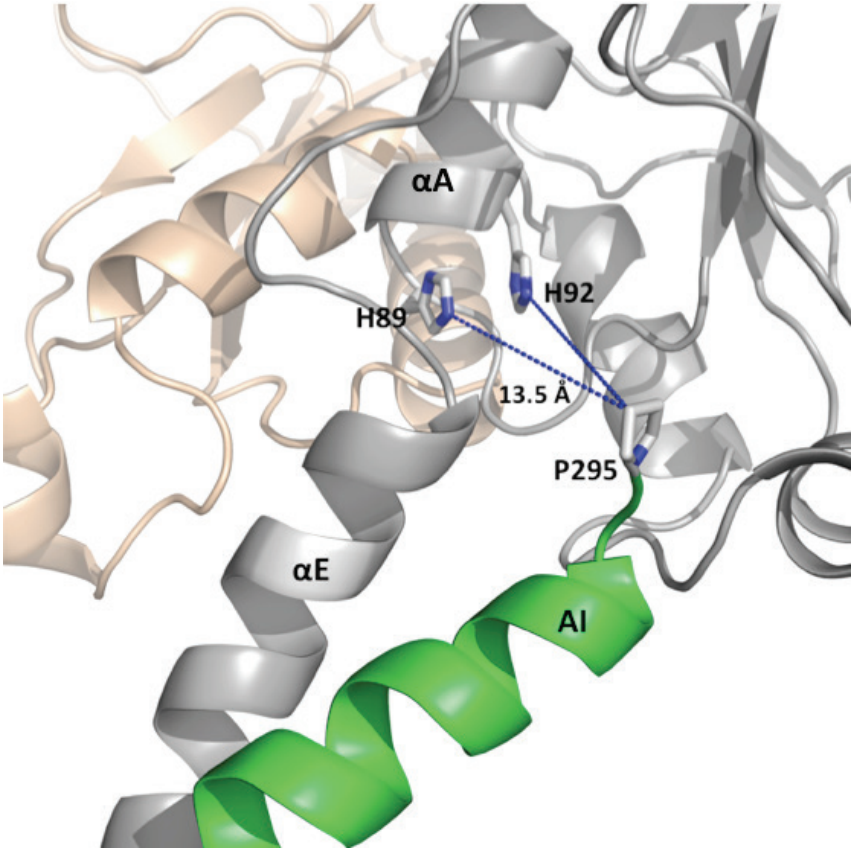

Figure 3.16 Distance between histidines in ^{89}HSGH^{92} site and P295.
P295 is 13.5 Å away from the H89 and H92. H89 and H92 are located on the HSGH motif in the active site and P295 is located at the end of the AI motif in domain M. This image was generated in PyMOL using PDB: 4MVC (CCT-312(Δ32)).

If the AI motif with the conjugated mBBr were to dock onto helix αE, it would reside within FRET distance of the transition metal ion and bimane's fluorescence would decline with the addition of increasing concentrations of Cu^{2+}. Figures 3.17 and 3.18 show that the fluorescence of bimane-modified CCT312-P295C was effectively reduced by Cu^{2+}.

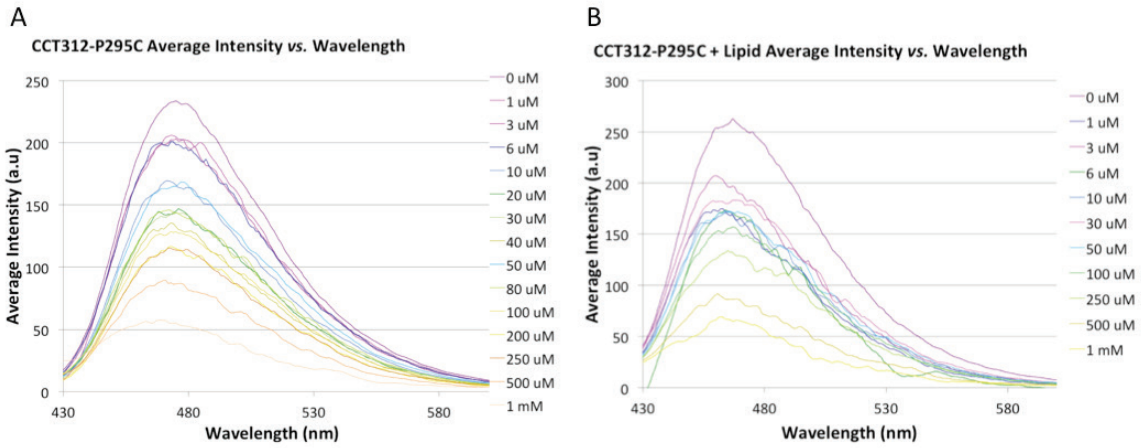

Figure 3.17 Effect of Cu^{2+} on the spectra of bimane-labeled CCT312-P295C.
Spectra of mBBr-reacted CCT312-P295C in the absence (A) or presence of 0.1 mM PC/PG vesicles (B) at increasing concentrations of Cu^{2+} ranging from 0 μM – 5 mM. The dye conjugated to the CCT312-P295C has an absorption/emission max of 394/470 nm. Bimane's emission decreases upon titration of metal.

One interpretation is that the AI motif and helix αE are within close proximity when the enzyme is silenced. In the presence of activating lipids, the AI motif dissociates from the active site as it inserts into the membrane bilayer, de-silencing the enzyme. The interaction of domain M with the lipid vesicles would decrease FRET. To explore this, I assessed the change in FRET upon addition of lipid vesicles to bimane-labeled CCT312-P295C. Figures 3.17B and 3.18 (red circles) show that the addition of activating lipids does not reduce the quenching effect. Both the quench curves (red and black traces, Figure 3.18) overlap, indicating that equivalent quenching by Cu^{2+} occurs in the presence or absence of lipids.

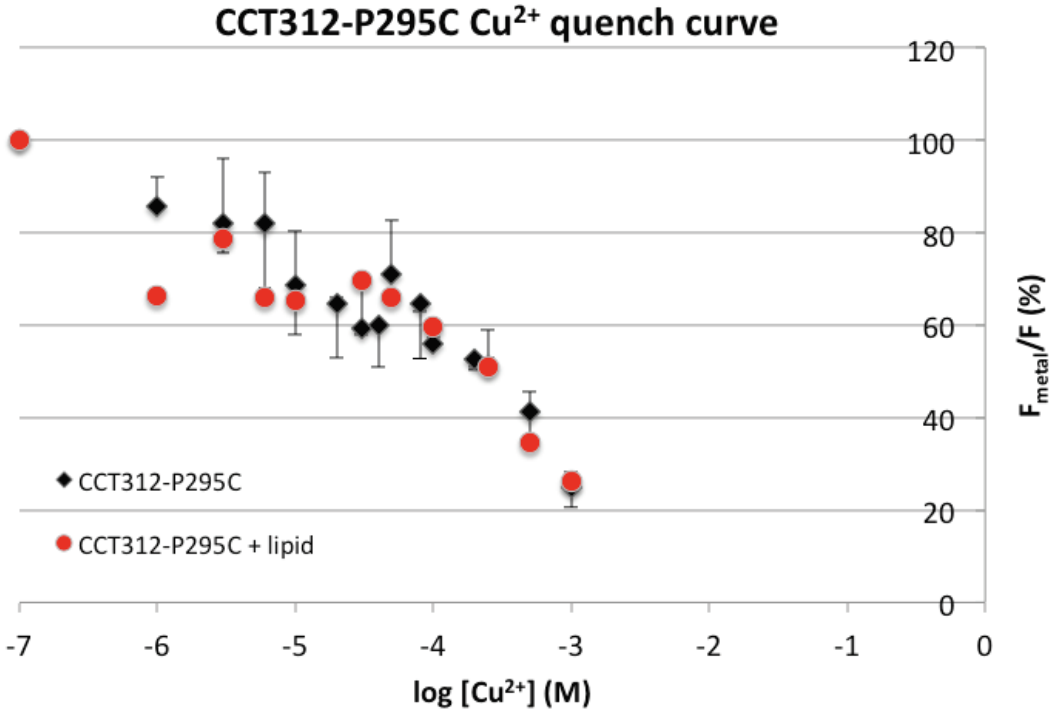

Figure 3.18 Cu^{2+} quenching of CCT312-P295C.
Average Cu^{2+} quenching of mBBr-reacted CCT312-P295C + 0.1 mM PC/PG vesicles (red) or – lipid (black). Increasing concentrations of Cu^{2+} ranging from 0 μM – 5 mM was added. The value, -7, on the X-axis denotes 0 μM (no Cu^{2+}). The results are averages of 2 replicates +/- standard error.

3.11. CCT312-P295C retained functional activity and bound to membranes

To confirm that the P295C mutation was not affecting the global protein fold, and to show that the P295C mutant was able to bind to membrane vesicles I conducted enzyme activity analyses on CCT312-P295C. I also tested the activity of this protein after mBBr conjugation. Both CCT312-P295C and mBBr-labeled CCT312-P295C had activities in the absence and presence of lipids that was undistinguishable from that of wild-type CCT (Figure 3.19). These results indicate that membrane binding, enzyme activity were not affected by the single cysteine mutation.

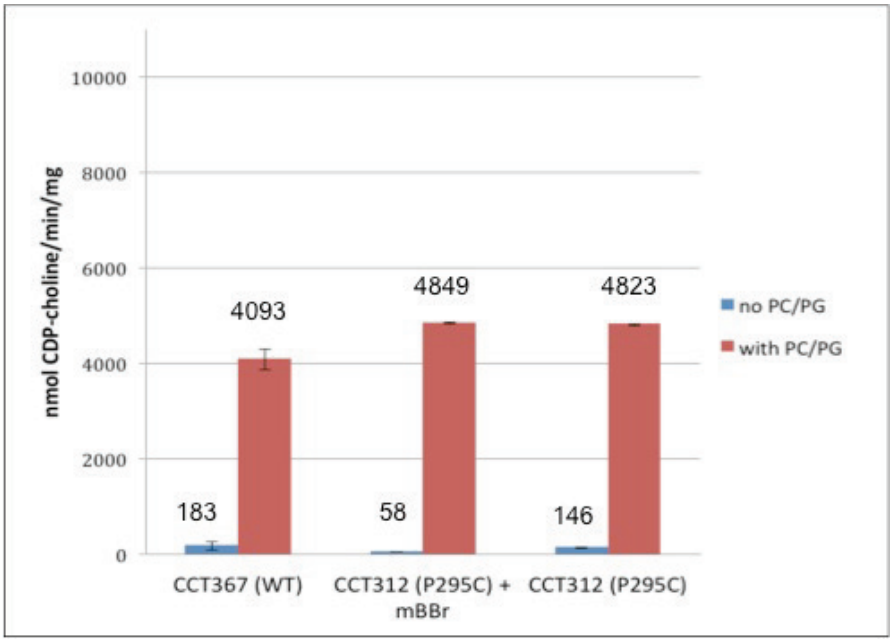

Figure 3.19 Specific activities of CCT constructs.
CCT367 Wild-type (WT), CCT312-P295C and mBBr-modified CCT312-P295C were assayed for activity with or without 0.1 mM PC/PG sonicated vesicles. The results are averages of 2 replicates +/- standard error.

In summary, the equivalent quench curves for CCT312-P295C with and without lipid binding reconfirm that the ^{89}HSGH^{92} site is not functioning as a metal-ion coordination site. The sharp decrease in fluorescence for all the labeled proteins at Cu^{2+} concentrations above 10^{-5} M is likely due to collisional quenching of bimane by Cu^{2+} ions in solution.

Chapter 4. Discussion

4.1. State of knowledge at the onset of my studies

The membrane binding domain, domain M, has a dual role in CCT regulation. It functions as a silencer in the enzyme's soluble state and an activator in the membrane-bound form. The evidence for the auto-inhibitory role of domain M is that truncation prior to domain M (CCT236) but not after results in partial constitutive (lipid-independent) activity of the enzyme. In the presence of lipids, domain M of full-length rat CCTα is displaced from the catalytic domain and the activity is elevated by ~3 fold compared to CCT236 (Ding, Taneva et al. 2012). At the onset of my research project, the mechanism by which domain M silences CCT activity was being studied. Photo-crosslinking between select sites on domains M and C combined with mass spectrometry and hydrogen-deuterium exchange experiments revealed that domain M docks onto a pair of amphipathic helices (αE) of the CCT dimer, at the base of the active site when CCT is not membrane-bound. These contacts were broken in the presence of activating lipid vesicles. A separate analysis of chimeric enzymes revealed that deletion of an ordered C-terminal 22-mer segment in domain M of rat CCT resulted in a loss of silencing function. Due to its silencing role, this segment is called the auto-inhibitory (AI) motif. The portion of domain M connecting the AI motif and helix αE showed characteristics of a disordered region when CCT was not membrane-engaged. Altogether these findings suggested that the AI motif is delivered to the base of the active site via a flexible leash to inhibit catalysis.

4.2. Rationale for the tmFRET project

To obtain additional evidence for this inhibitory interaction, I turned to transition metal ion FRET (tmFRET), which offers several advantages over crystallography or

NMR spectroscopy: the technique can be applied to proteins of any size, membrane proteins or even on single molecules (J.W., Puljung et al. 2009). In addition to measuring intramolecular distances, tmFRET can also provide information about the structure and conformational changes of proteins in their native environment. The tmFRET analysis was expected to provide distances between the AI motif and the active site in the soluble inhibited CCT form as well as confirm that this contact is broken upon membrane binding of domain M. Once the methodology was established, the goal was to use tmFRET-derived distance changes to assess the role of specific residues, targeted by mutagenesis, in the αE and AI helices contributing to the silencing interaction.

Towards the end of my masters' project, a 3.0 Å structure of CCT-312(Δ32) containing the catalytic domain and the AI motif of domain M was solved (Lee, Taneva et al. 2014), confirming an interaction between the AI and αE helices (Figure. 4.1). The two AI helices dock in an anti-parallel fashion onto the αE helix pair to form a stable four-helix bundle, in which the C-terminus of the AI motif forms a sharp turn at the entrance to the active site and makes an unanticipated close interaction with loop L2 housing Lys122. This new structural information provided insight into logical positions for engineering mBBr conjugation sites for analysis of potential FRET interactions between the AI helix-turn and the catalytic domain.

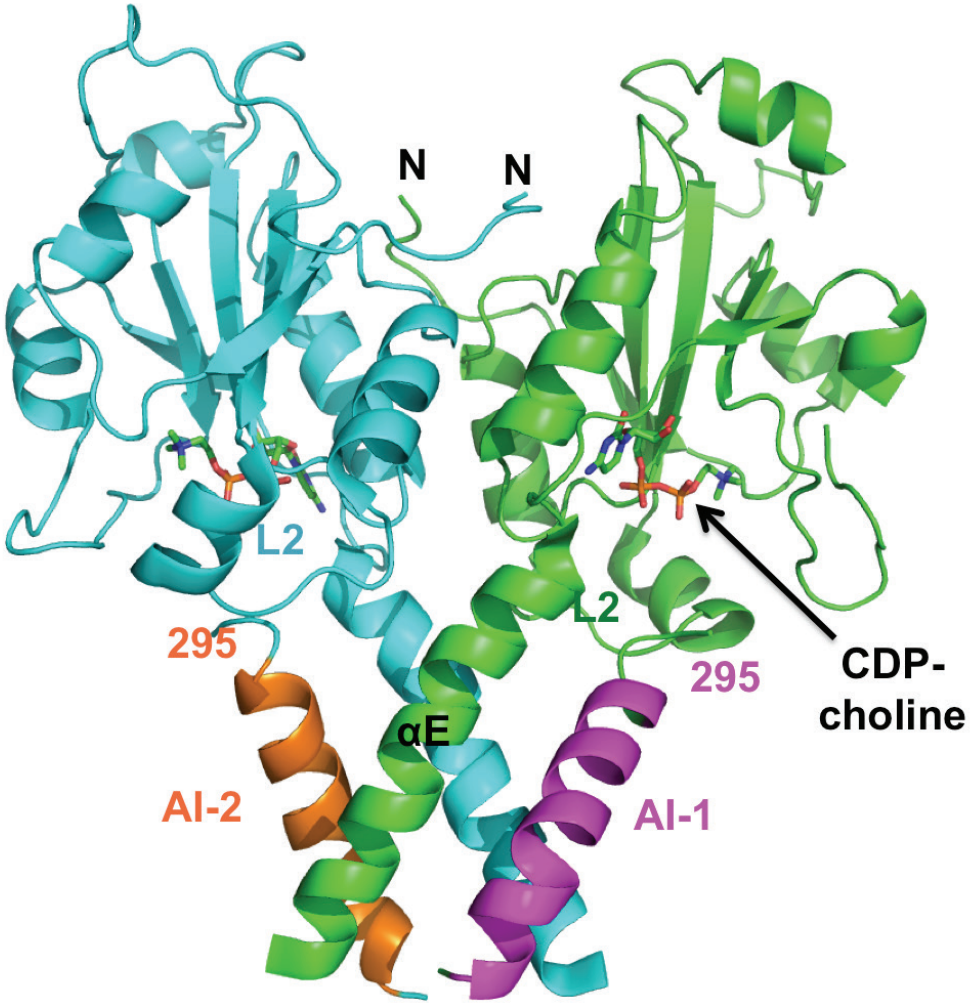

Figure 4.1 Structure of CCT-312(Δ32).
This structure of CCT-312(Δ32) missing residues 238-269, shows both the catalytic and a portion of the membrane-binding domain. CDP-choline is shown in stick representation. The AI segment (residues 275-295) of domain M interacts closely with helix αE and loop L2 in the active site. The linkers between the end of the αE helices and the start of the AI helices are unresolved. This figure was generated in PyMOL using PDB: 4MVC.

4.3. Analysis of tmFRET results for CCT

I explored the potential for the native di-histidine motif (^{89}HSGH^{92}) in the CCT active site as a site for metal ion coordination and utility as a FRET acceptor. As the

FRET donor site, I initially used a site in helix αE (C207), and later a site in the AI helix-turn (C295). The experiments described in chapter 3 suggested that fluorescence quenching of bimane conjugated to either of two sites within potential tmFRET distance of the di-histidine site, was collisional rather than FRET-based. Quenching was not significantly affected by agents that should have inhibited Cu^{2+} chelation to the HSGH site in CCT or manipulations that increased the distance between donor and putative acceptor.

Yu and colleagues conducted tmFRET experiments to study the structure and conformational changes in maltose binding protein (MBP) upon ligand binding (Yu, Wu et al. 2013). For each single-cysteine, dye-conjugated MBP that they studied, fluorescence quenching of constructs with and without the di-histidine metal-binding site (control) were compared. For constructs with the di-histidine motif, the quenching was two-component (Figure 4.2A). FRET-based quenching (solid trace) occurred at nanomolar concentrations (10^{-8} to 10^{-6} M) of Cu^{2+}. Fluorophore quenching observed at higher metal concentrations (near and above 10^{-5} M) was ascribed to collisional quenching (dotted trace), since this quenching was observed when the FRET acceptor site was absent. In contrast, Taraska and colleagues reported that collisional quenching occurred above10^{-3} M of Cu^{2+} (Fig. 4.2B). The differing range for collisional quenching should be a function of the solvent accessibility of the conjugated fluorophore. However, the authors of these papers did not provide a rationale for the discrepant metal ion concentration ranges for collisional quenching observed for peptides *vs* the protein, MBP.

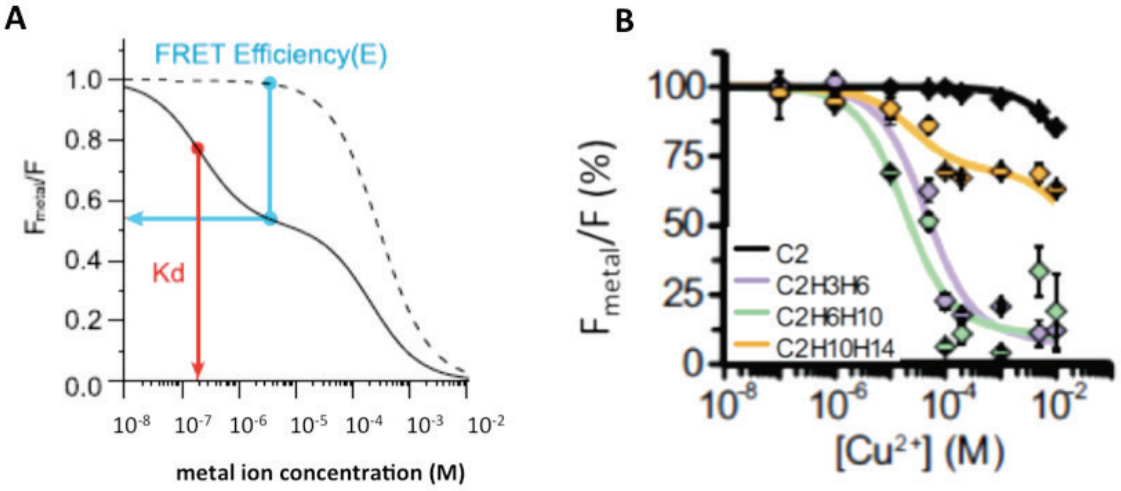

Figure 4.2 FRET-based quenching *vs*. collisional quenching.
(A) Fluorescence quenching has two components: FRET-based quenching and collisional quenching. Quenching at high metal concentrations ($\geq 10^{-5}$ M or above) is due to collisional quenching (dotted trace using protein lacking di-histidine motif). Quenching between 10^{-8} – 10^{-6} M of metal ion is due to tmFRET (solid trace using protein with di-histidine motif). This figure is from (Yu et al. 2013), Figure 2C. (B) Cu^{2+} quenching of monobromobimane conjugated at fixed distances from engineered HXXH or HXXXH sites in short 16-aa-α-helical model peptides. The black curve has no functional di-histidine site and thus demonstrates strictly collisional quenching, which does not occur until > 10^{-3} M Cu^{2+}. This figure is from (Taraska, Puljung et al. 2009), Figure 1F.

The quench curves I obtained for CCT look very similar to the quenching effect observed for the control in figure 4.2A, lacking the di-histidine motif. My quench curves only depict the second component, reduced fluorescence above 10^{-5} M. One caveat to my analyses is that insufficient fluorescence data was collected at Cu^{2+} concentrations below 10^{-6} M. Thus the "plateau" regions at the low [Cu^{2+}] end of the quench curves were noisy, blurring any potential differences between control and test quenching results. Definitive conclusions regarding FRET would be facilitated by additional data at sub-micro molar concentrations of Cu^{2+}.

How certain can one be about the lack of FRET in the CCT analyses? Working with the full-length CCT construct, I found little difference in the quench curves carried out at pH 6, a pH expected to protonate the histidines in the ^{89}HSGH^{92} motif. However, since the environment surrounding the HSGH site is highly electro-positive, one could argue that this could cause an apparent pKa shift in which the histidines remain deprotonated even at a bulk pH of 6.0. The lack of effect of CDP-choline could be

explained by highly effective competition with Cu^{2+}. Lastly, the serine replacing the histidine at residue 89 of the HSGH site might have substituted its oxygen as a replacement for the ε-nitrogen of the histidines in coordinating the Cu^{2+}. Although I present these arguments as caveats, it is more likely that all three negative results are indicative of an absence of an operating FRET acceptor at the HSGH site. The final test of this site involved elimination of FRET potential by complete dissociation of the AI motif from the catalytic domain by membrane binding. This also had no effect on the quench curve, supporting the argument for a non-functional site at HSGH. Below I evaluate the possible reasons for the lack of FRET.

4.4. Reasons for a non-functioning HSGH site as a tmFRET acceptor

4.4.1. Distance requirement for tmFRET and the path connecting donor-acceptor pairs

tmFRET is effective within distances of 5-20 Å. I initially tested tmFRET between bimane conjugated to an engineered cysteine at position 207 on helix αE and Cu^{2+} bound to the native histidines in the HSGH motif. In the solved structure of CCT236 (PDB ID: 3HL4), the ε-nitrogen of H89 and H92 are respectively 12 Å and 14 Å away from the T207 hydroxyl group in helix αE (Figure 3.1, Chapter 3). This falls within the distance requirement of tmFRET (Taraska, Puljung et al. 2009). There are polypeptide residues in the path connecting C207 and the di-histidines. An obvious concern was if these intervening residues would affect tmFRET measurements.

tmFRET is a through-space excitation energy transfer process that is mostly independent of intervening solvent or macromolecules (Lackowicz, 2006). While examining conformational changes in the HCN channel upon cAMP binding to the cyclic nucleotide-binding domain (CNBD), Taraska and colleagues observed FRET even when the path connecting the donor and acceptor was not barrier-free (J.W., Puljung et al. 2009). To understand the structural changes in the C-helix (CNBD) and C-linker (linker to HCN) upon cAMP binding, cysteines were engineered in the F'-helix (N520C) of the C-linker or in the β-roll (K570C) of the CNBD. These cysteines were modified with

fluorescein (FRET donor). Nickel binding motifs were engineered at four different positions along the C-helix. One of the binding sites has two histidines at position 630 and 634. As can be seen in figure 4.3, the path between Ni^{2+} and fluorescein is barrier free to C520 but not to C570. However, the authors reported observing FRET (37.4%) between fluorescein conjugated to C570 and Ni^{2+} bound to H630 and H634. Therefore, based on these findings I was hopeful that I would be able to measure FRET between helix αE and the di-histidine motif in CCT.

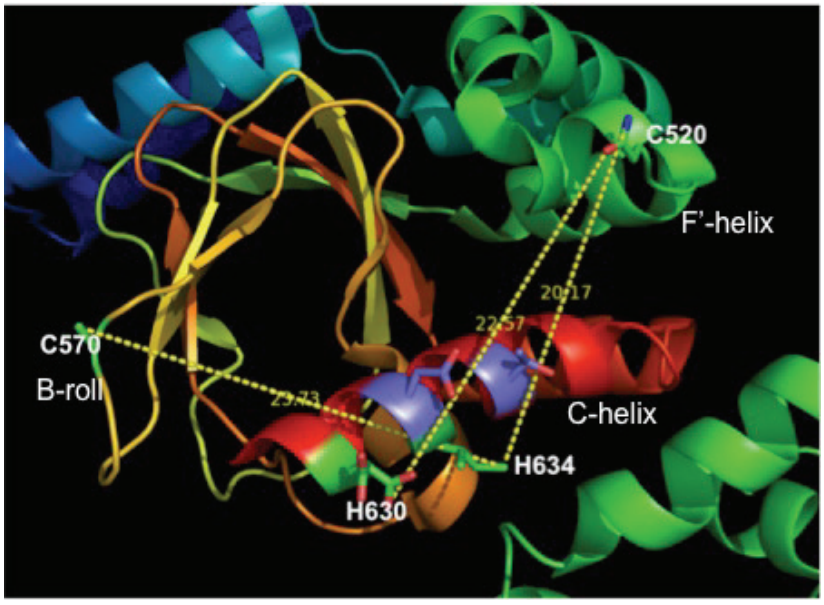

Figure 4.3 Path between FRET donor-acceptor pairs in the HCN2 ion channel.
The path between the di-histidines (H630 and H634) on the C-helix (CNBD) and C520 in the F'-helix (C-linker) is barrier free whereas there are intervening polypeptide residues between the di-histidines and C570 in the β-roll (CNBD). This figure was generated in PyMOL using PDB: 3FFQ.

After the structure of CCT-312(Δ32) was solved I probed interactions between the AI motif and catalytic domain in CCT by switching the mBBr conjugation site from C207 to C295 at the end of the AI motif. In this case, there is a barrier-free path separated by 13.5 Å connecting C295 and the di-histidine motif (Figure 3.16, Chapter 3). Therefore, the lack of FRET between bimane at C295 and the putative Cu^{2+} binding site at HSGH cannot be ascribed to intervening barriers. This leaves open the possibility that the native histidines in the HSGH motif of CCT do not serve as a good site for Cu^{2+} binding. I provide possible reasons for this occurrence in the succeeding sections

4.4.2. Metal binding is highly dependent on the spacing of histidines along an α-helix

Pairs of histidines spaced one turn away on α-helices have been shown to coordinate transition metal ions such as Cu^{2+} or Ni^{2+} (Taraska, Puljung et al. 2009, Taraska, Puljung et al. 2009). The δ or ε nitrogens of the imidazole groups from both histidines are involved in forming a ternary complex with a single metal ion. In CCT, the HSGH motif is located at the start of helix αA following the L1 loop (Figure 4.4).

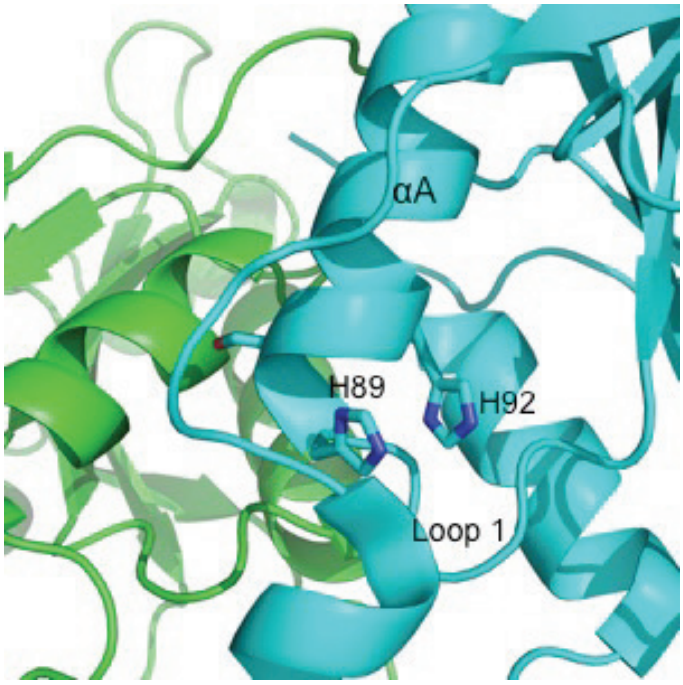

Figure 4.4 Location of ^{89}HSGH^{92} motif.
The HSGH motif is located in helix αA, following loop L1 in CCT's catalytic domain. This figure was generated in PyMOL using PDB: 3HL4 (CCT236).

One helical turn consists of 3.6 residues. Thus, either an *i* +3 or an *i* +4 spacing between histidines in an α-helix can potentially form a binding site for a metal ion. It is possible that the *i* + 3 spacing of the histidine residues within the HSGH motif did not provide the right geometry for Cu^{2+} binding. The geometric requirements for metal chelation in proteins are highly specific. Common secondary elements such as alpha helices and β sheets found within proteins help provide the specific geometric framework and scaffolding required for metal binding. Modeling calculations have shown that the following di-histidine configurations in secondary elements of proteins form proper

chelating sites for a Cu^{2+} ion: His-X_3-His in an α-helix, His-X_2-His in a reverse β turn and His-X-His in a β strand (Arnold and Haymore 1991). Since there are two intervening residues instead of three separating H89 and H92 in helix αA, the histidines might be too close for Cu^{2+} conjugation. An *i* +4 spacing might have created a better binding site for the metal. Previously, tmFRET experiments conducted on short α-helical model peptides indicated that both Cu^{2+} and Ni^{2+} preferentially bound with a higher affinity to the *i* + 4 configuration as opposed to the *i* +3 configuration (Taraska, Puljung et al. 2009) . FRET was observed in both cases, however bimane quenching occurred only at much higher concentrations of metal for peptides with the *i* + 3 spacing.

In the two crystal structures of CCT, the N-ε2 (Figure 4.5) of the histidines are spaced ~3.5 Å apart, bringing the histidine side chains on helix αA into close spatial proximity. This configuration is most likely adopted for the interaction of the HSGH motif with the substrate, CTP. However it is also within the range of the spacing of histidines forming Cu^{2+}-binding sites in the structures of solved proteins (3 – 4.2 Å) (Ryvkin and Greenaway 2010). The first histidine, H89, is located at the start of an alpha helix following a loop, which may allow the histidine to change conformation.

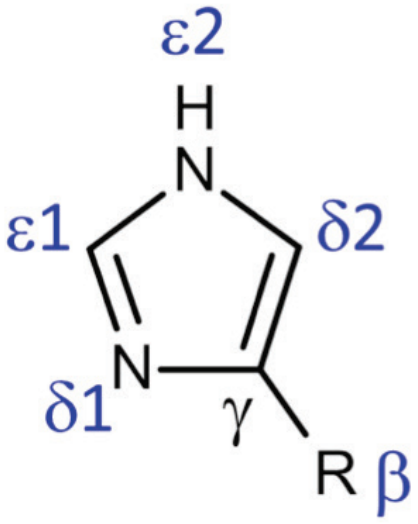

Figure 4.5 Imidazole sidechain of histidine.
The imidazole ring of histidine is aromatic. It has two nitrogen atoms labeled δ1 and ε2. In the nonionized state, the hydrogen atom is on the ε2 nitrogen atom. Protonation of δ1 creates a positive charge and antagonizes metal chelation.

4.4.3. Cu^{2+} access to metal-binding site

In addition to the spacing of histidines, solvent exposure can also affect the affinity of the di-histidine site for the metal ion. Surface-exposed histidines are well suited for metal coordination. A surface representation of CCT in PyMOL shows that the HSGH motif (pink) is buried in the active site pocket of the enzyme and is not very solvent-accessible (Figure 4.5). The low Cu^{2+} affinity suspected from my results could be related to the limited accessibility.

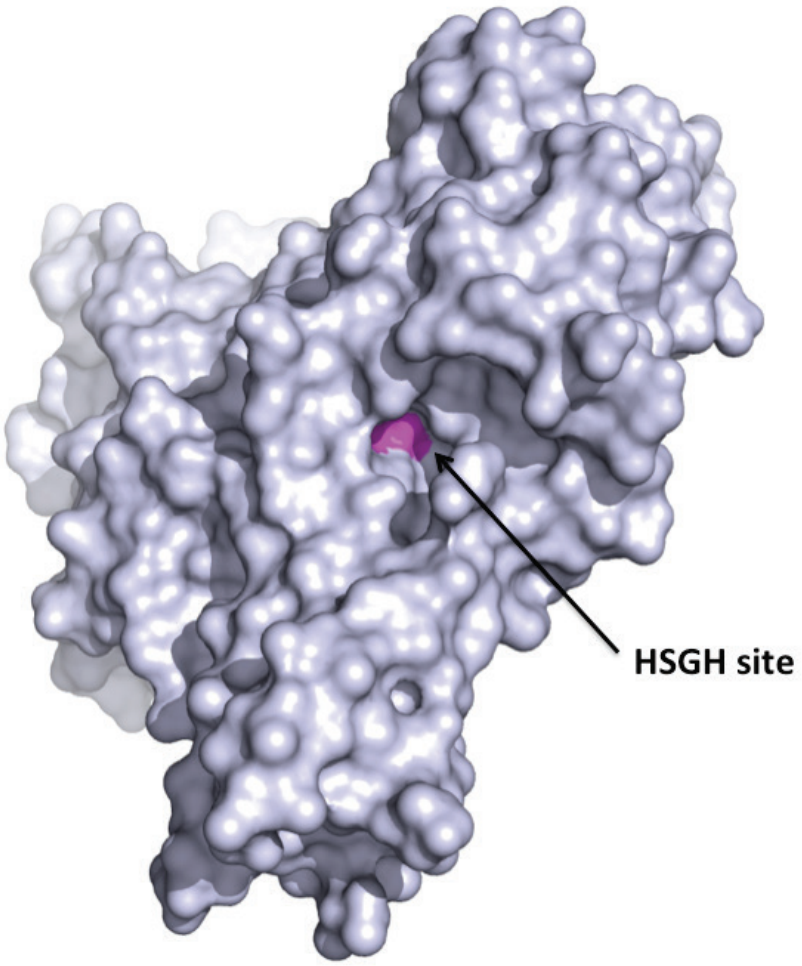

Figure 4.6 Surface representation of CCT-312(Δ32).
The HSGH site, highlited in pink, is buried and not very solvent-accessible. This figure was generated in PyMOL using PDB: 4MVC.

4.4.4. The electrostatic environment around the HSGH motif

The metal-binding ability or strength of a chelating site is sensitive to the surrounding environmental conditions. Figure 4.6 shows an electrostatic potential map of the molecular surface of CCT. The HSGH motif is surrounded by many polar, positively charged residues (blue shade). The entryway to the active site is flanked by Lys122 and Arg196. It is possible that these positively charged residues prevent Cu^{2+} from binding to the histidines as they create strong electrostatic repulsion.

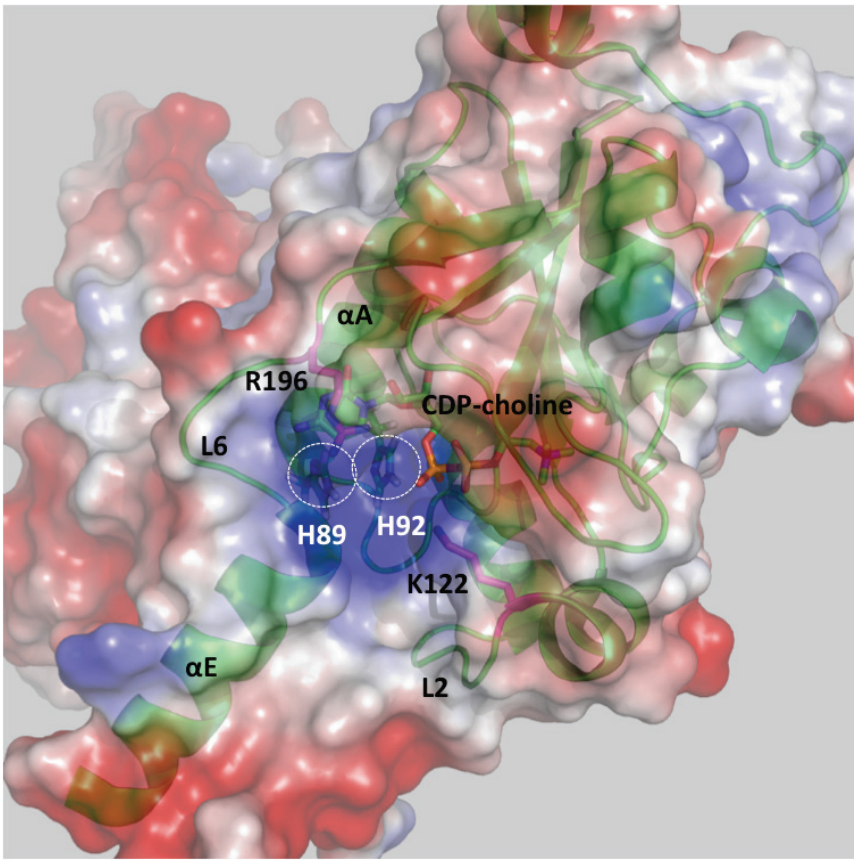

Figure 4.7 Electrostatic potential map of CCT.
The surface electrostatic potential of CCT shows that the HSGH site and surrounding area are highly positively charged (blue). This figure was generated in PyMOL using vaccum electrostatics as the default option (PDB: 3HL4). This view is similar to that displayed in figure 4.6.

4.5. Future directions

The new 3.0 Å crystal structure of CCT-312(Δ32) provided evidence for loop L2 as a potential target of auto-inhibition by the AI motif (Lee, Taneva et al. 2014). Loop L2

is mobile during a catalytic cycle. It houses the key catalytic residue, Lys-122, which likely undergoes different orientations during a catalytic cycle. Molecular dynamics simulations of CCT-312(Δ32) with and without the AI helix showed that AI helix-loop L2 interactions constrain Lys-122 orientations and reduce the fluctuations in loop L2 (Lee, Taneva et al. 2014).

Transition metal ion FRET can be used to probe the AI-turn-L2 interactions. In the future, bimane can be conjugated to a cysteine residue on the AI helix and di-histidines can be engineered on helix αB adjacent to loop L2. Upon addition of metal ion, the quenching of bimane would be observed only when the AI is bound. Mutagenesis of residues in the αE, AI and L2 loop are being prepared to examine the contributions of individual amino acids to catalytic silencing by this ternary interaction. FRET between this donor-acceptor pair could then be examined as a measure of the strength of the AI interaction, and these measurements would be correlated with the extent of enzymatic inhibition.

References

Arnold, F. H. and B. L. Haymore (1991). "Engineered metal-binding proteins: purification to protein folding." Science **252**(5014): 1796-1797.

Arnold, R. S., A. A. DePaoli-Roach and R. B. Cornell (1997). "Binding of CTP:phosphocholine cytidylyltransferase to lipid vesicles: diacylglycerol and enzyme dephosphorylation increase the affinity for negatively charged membranes." Biochemistry **36**(20): 6149-6156.

Bogan, M. J., G. R. Agnes, F. Pio and R. B. Cornell (2005). "Interdomain and membrane interactions of CTP:phosphocholine cytidylyltransferase revealed via limited proteolysis and mass spectrometry." J Biol Chem **280**(20): 19613-19624.

Bork, P., L. Holm, E. V. Koonin and C. Sander (1995). "The cytidylyltransferase superfamily: identification of the nucleotide-binding site and fold prediction." Proteins **22**(3): 259-266.

Chong, S. S., S. G. Taneva, J. M. Lee and R. B. Cornell (2014). "The curvature sensitivity of a membrane-binding amphipathic helix can be modulated by the charge on a flanking region." Biochemistry **53**(3): 450-461.

Cornell, R. B. and I. C. Northwood (2000). "Regulation of CTP:phosphocholine cytidylyltransferase by amphitropism and relocalization." Trends Biochem Sci **25**(9): 441-447.

Cowan-Jacob, S. W., G. Fendrich, P. W. Manley, W. Jahnke, D. Fabbro, J. Liebetanz and T. Meyer (2005). "The crystal structure of a c-Src complex in an active conformation suggests possible steps in c-Src activation." Structure **13**(6): 861-871.

Craig, L., J. E. Johnson and R. B. Cornell (1994). "Identification of the membrane-binding domain of rat liver CTP:phosphocholine cytidylyltransferase using chymotrypsin proteolysis." J Biol Chem **269**(5): 3311-3317.

Davies, S. M., R. M. Epand, R. Kraayenhof and R. B. Cornell (2001). "Regulation of CTP: phosphocholine cytidylyltransferase activity by the physical properties of lipid membranes: an important role for stored curvature strain energy." Biochemistry **40**(35): 10522-10531.

Dennis, M. K., S. G. Taneva and R. B. Cornell (2011). "The intrinsically disordered nuclear localization signal and phosphorylation segments distinguish the membrane affinity of two cytidylyltransferase isoforms." J Biol Chem **286**(14): 12349-12360.

Ding, Z., S. G. Taneva, H. Huang, S. A. Campbell, L. Semenec, N. Chen and R. B. Cornell (2012). "A 22-mer segment in the structurally pliable regulatory domain of metazoan CTP: phosphocholine cytidylyltransferase facilitates both silencing and activating functions." J Biol Chem **287**: 38980-38991.

Dunne, S. J., R. B. Cornell, J. E. Johnson, N. R. Glover and A. S. Tracey (1996). "Structure of the membrane binding domain of CTP:phosphocholine cytidylyltransferase." Biochemistry **35**(37): 11975-11984.

Exton, J. H. (1990). "Signaling through phosphatidylcholine breakdown." J Biol Chem **265**(1): 1-4.

Fiscus, W. G. and W. C. Schneider (1966). "The role of phospholipids in stimulating phosphorylcholine cytidyltransferase activity." J Biol Chem **241**(14): 3324-3330.

Friesen, J. A., H. A. Campbell and C. Kent (1999). "Enzymatic and cellular characterization of a catalytic fragment of CTP:phosphocholine cytidylyltransferase alpha." J Biol Chem **274**(19): 13384-13389.

Gluzman, Y. (1981). "SV40-transformed simian cells support the replication of early SV40 mutants." Cell **23**(1): 175-182.

Goerke, J. (1998). "Pulmonary surfactant: functions and molecular composition." Biochim Biophys Acta **1408**(2-3): 79-89.

Helmink, B. A., J. D. Braker, C. Kent and J. A. Friesen (2003). "Identification of lysine 122 and arginine 196 as important functional residues of rat CTP:phosphocholine cytidylyltransferase alpha." Biochemistry **42**(17): 5043-5051.

Huang, H. K., S. G. Taneva, J. Lee, L. P. Silva, D. C. Schriemer and R. B. Cornell (2013). "The membrane-binding domain of an amphitropic enzyme suppresses catalysis by contact with an amphipathic helix flanking its active site." J Mol Biol **425**: 1546-1564.

Huang, H.K. (2011). Mechanism of silencing the catalytic domain by the regulatory membrane lipid binding domain of an amphitropic cytidylyltransferase. In Molecular Biology and Biochemistry (Burnaby, B.C., Simon Fraser University), pp. 1-120.

J.W., T., M. C. Puljung, N. B. Olivier, G. E. Flynn and W. N. Zagotta (2009). "Mapping the structure and conformational movements of proteins with transition metal ion FRET." Nature Methods **6**: 532-537.

Jackowski, S. and P. Fagone (2005). "CTP: Phosphocholine cytidylyltransferase: paving the way from gene to membrane." J Biol Chem **280**(2): 853-856.

Johnson, J. E., M. Xie, L. M. Singh, R. Edge and R. B. Cornell (2003). "Both acidic and basic amino acids in an amphitropic enzyme, CTP:phosphocholine cytidylyltransferase, dictate its selectivity for anionic membranes." J Biol Chem **278**(1): 514-522.

Kalmar, G. B., R. J. Kay, A. Lachance, R. Aebersold and R. B. Cornell (1990). "Cloning and expression of rat liver CTP: phosphocholine cytidylyltransferase: an amphipathic protein that controls phosphatidylcholine synthesis." Proc Natl Acad Sci U S A **87**(16): 6029-6033.

Kay, R. and Humphries, R.K. New Vectors and Procedures for Isolating cDNAs Encoding Cell Surface Proteins by Expression Cloning in COS cells. Methods in Molecular and Cellular Biology **2**, 254-265 (1991).

Kent, C. (1997). "CTP:phosphocholine cytidylyltransferase." Biochimica et Biophysica Acta (BBA) - Lipids and Lipid Metabolism **1348**(1–2): 79-90.

Leatherbarrow, R. J., A. R. Fersht and G. Winter (1985). "Transition-state stabilization in the mechanism of tyrosyl-tRNA synthetase revealed by protein engineering." Proc Natl Acad Sci U S A **82**(23): 7840-7844.

Lee, J., J. Johnson, Z. Ding, M. Paetzel and R. B. Cornell (2009). "Crystal structure of a mammalian CTP: phosphocholine cytidylyltransferase catalytic domain reveals novel active site residues within a highly conserved nucleotidyltransferase fold." J Biol Chem **284**(48): 33535-33548.

Lee, J., S. Taneva, B. Holland, D. Tieleman and R. Cornell (2014). "Structural Basis for Autoinhibition of CTP:Phosphocholine Cytidylyltransferase (CCT), the Regulatory Enzyme in Phosphatidylcholine Synthesis, by Its Membrane-binding Amphipathic Helix." J Biol Chem **289**(3): 1742-1755.

MacDonald, J. I. and C. Kent (1994). "Identification of phosphorylation sites in rat liver CTP: phosphocholine cytidylyltransferase." J Biol Chem **269**(14): 10529-10537.

Park, Y. S., P. Gee, S. Sanker, E. J. Schurter, E. R. Zuiderweg and C. Kent (1997). "Identification of functional conserved residues of CTP:glycerol-3-phosphate cytidylyltransferase. Role of histidines in the conserved HXGH in catalysis." J Biol Chem **272**(24): 15161-15166.

Pattridge, K. A., C. H. Weber, J. A. Friesen, S. Sanker, C. Kent and M. L. Ludwig (2003). "Glycerol-3-phosphate cytidylyltransferase. Structural changes induced by binding of CDP-glycerol and the role of lysine residues in catalysis." J Biol Chem **278**(51): 51863-51871.

Pufall, M. A. and B. J. Graves (2002). "Autoinhibitory domains: modular effectors of cellular regulation." Annu Rev Cell Dev Biol **18**: 421-462.

Ryvkin, F. and F. T. Greenaway (2010). "Modeling Cu(II) binding to peptides using the extensible systematic force field." Bioinorg Chem Appl **2010**: 724210.

Stinson, B. M., A. R. Nager, S. E. Glynn, K. R. Schmitz, T. A. Baker and R. T. Sauer (2013). "Nucleotide binding and conformational switching in the hexameric ring of a AAA+ machine." Cell **153**(3): 628-639.

Taneva, S., M. K. Dennis, Z. Ding, J. L. Smith and R. B. Cornell (2008). "Contribution of each membrane binding domain of the CTP:phosphocholine cytidylyltransferase-alpha dimer to its activation, membrane binding, and membrane cross-bridging." J Biol Chem **283**(42): 28137-28148.

Taneva, S., J. E. Johnson and R. B. Cornell (2003). "Lipid-induced conformational switch in the membrane binding domain of CTP:phosphocholine cytidylyltransferase: a circular dichroism study." Biochemistry **42**(40): 11768-11776.

Taraska, J. W., M. C. Puljung, N. B. Olivier, G. E. Flynn and W. N. Zagotta (2009). "Mapping the structure and conformational movements of proteins with transition metal ion FRET." Nature Methods **6**: 532-537.

Taraska, J. W., M. C. Puljung and W. N. Zagotta (2009). "Short-distance probes for protein backbone structure based on energy transfer between bimane and transition metal ions." Proc Natl Acad Sci U S A **106**: 16227-16232.

Tsukagoshi, Y., J. Nikawa and S. Yamashita (1987). "Molecular cloning and characterization of the gene encoding cholinephosphate cytidylyltransferase in Saccharomyces cerevisiae." Eur J Biochem **169**(3): 477-486.

Veitch, D. P. and R. B. Cornell (1996). "Substitution of serine for glycine-91 in the HXGH motif of CTP:phosphocholine cytidylyltransferase implicates this motif in CTP binding." Biochemistry **35**(33): 10743-10750.

Veitch, D. P., D. Gilham and R. B. Cornell (1998). "The role of histidine residues in the HXGH site of CTP:phosphocholine cytidylyltransferase in CTP binding and catalysis." Eur J Biochem **255**(1): 227-234.

Wang, Y. and C. Kent (1995). "Effects of altered phosphorylation sites on the properties of CTP:phosphocholine cytidylyltransferase." J Biol Chem **270**(30): 17843-17849.

Wang, Y. and C. Kent (1995). "Identification of an inhibitory domain of CTP:phosphocholine cytidylyltransferase." J Biol Chem **270**(32): 18948-18952.

Wang, Y., J. I. MacDonald and C. Kent (1995). "Identification of the nuclear localization signal of rat liver CTP:phosphocholine cytidylyltransferase." J Biol Chem **270**(1): 354-360.

Weber, C. H., Y. S. Park, S. Sanker, C. Kent and M. L. Ludwig (1999). "A prototypical cytidylyltransferase: CTP:glycerol-3-phosphate cytidylyltransferase from bacillus subtilis." Structure **7**(9): 1113-1124.

Weinhold, P. A., M. E. Rounsifer and D. A. Feldman (1986). "The purification and characterization of CTP:phosphorylcholine cytidylyltransferase from rat liver." J Biol Chem **261**(11): 5104-5110.

Wilgram, G. F. and E. P. Kennedy (1963). "INTRACELLULAR DISTRIBUTION OF SOME ENZYMES CATALYZING REACTIONS IN THE BIOSYNTHESIS OF COMPLEX LIPIDS." J Biol Chem **238**: 2615-2619.

Xie, M., J. L. Smith, Z. Ding, D. Zhang and R. B. Cornell (2004). "Membrane binding modulates the quaternary structure of CTP:phosphocholine cytidylyltransferase." J Biol Chem **279**(27): 28817-28825.

Yang, E. and H. Schulman (1999). "Structural examination of autoregulation of multifunctional calcium/calmodulin-dependent protein kinase II." J Biol Chem **274**(37): 26199-26208.

Yu, X., X. Wu, G. A. Bermejo, B. R. Brooks and J. W. Taraska (2013). "Accurate high-throughput structure mapping and prediction with transition metal ion FRET." Structure **21**(1): 9-19.

Appendix A.

QuikChange Site-Directed Mutagenesis

Table A1 QuikChange Site-directed mutagenesis conditions for CCT312 mutants

Construct	DNA polymerase	Cycling parameter	Competent cell for transformation
pET24a-CCT312-H89S-T207C	*Pfu* DNA polymerase	1 cycle of heating for 30 s at 95°C and 16 cycles of heating for 30 s at 95°C, 1 min at 55°C and 7 min at 72°C	NovaBlue
pET24a-CCT312-H89A-T207C	*Pfu* DNA polymerase	1 cycle of heating for 30 s at 95°C and 16 cycles of heating for 30 s at 95°C, 1 min at 55°C and 7 min at 72°C	NovaBlue
pET24a-CCT312-P295C	Phusion DNA polymerase	1 cycle of heating for 30 s at 95°C and 18 cycles of heating for 30 s at 95°C, 1 min at 55°C and 7 min at 72°C	DH5α

Appendix B

Oligonucleotide primers

Primer sequence to generate pET24a-CCT312-H89S-T207C

Template: pET24a-CCT312-T207C

Codon	83	84	85	86	87	88	89	90	91	92	93	94
	gly	ile	phe	asp	leu	phe	ser	ser	gly	his	ala	arg

Sense 5' - GGA ATA TTT GAC TTG TTT **AGC** TCT GGT CAT GCC CGG - 3'

Antisense 3' – CCT TAT AAA CTG AAC AAA **TCG** AGA CCA GTA CGG GCC – 5'

Primer sequence to generate pET24a-CCT312-H89A-T207C

Template: pET24a-CCT312-H89S-T207C

Ser

Primers: **AGC (Template)**

Forward: 5' GGA ATA TTT GAC TTG TTT **GCC** TCT GGT CAT GGC CGG -3'

gly ile phe asp leu phe ala ser gly his ala arg

^{83}G ^{84}I ^{85}F ^{86}D ^{87}L ^{88}F ^{89}A ^{90}S ^{91}G ^{92}H ^{93}A ^{94}R

Reverse: 5' CCG GCC ATG ACC AGA **GGC** AAA CAA GTC AAA TAT TCC -3'

Primer sequence to generate pET24a-CCT312-P295C

Step 1. Prepare pET24a-CCT-312 (cysless)

Change C207 back to T207 by QuikChange site-directed mutagenesis

Template: pET24a-CCT312-T207C

Cys

Primers **TGC (Template)**

Forward: 5' CC ACA TCA GAC ATC ATC **ACC** CGC ATT GTC CGT GAC **3'**

^{202}T S D I I ^{207}T R I V R D

Reverse: 5' GTC ACG GAC AAT GCG **GGT** GAT GAT GTC TGA TGT GG **3'**

Step 2. Prepare pET24a-CCT312-P295C

Template: pET24a-CCT312 (cysless) (Prepared in step 1).

Pro

Primers **CCA (Template)**

Forward: 5' CTG GAA ATG TTT GGT **TGC** GAA GGA GCG CTG AAG **3'**

^{290}L E M F G ^{295}C E G A L K

Reverse: 5' CTT CAG CGC TCC TTC **GCA** ACC AAA CAT TTC CAG **3'**

Appendix C.

Expression and purification conditions for CCT312 constructs

Table C1 Expression and purification conditions for CCT312 mutants.

Protein	Culture volume for expression (ml)	Lysis buffer volume (ml)	Wash buffer volume (ml)	Volume of 6M GuHCl (ml)	Elution volume for purification (ml)
CCT312-T207C	100 ml x 2	10 ml	6 ml	6 ml	3 ml
CCT312-H89S-T207C	100 ml x 2	10 ml	6 ml	6 ml	3 ml
CCT312-P295C	200 ml x 2	20 ml	12 ml	12 ml	1.5 ml